Hyperfine-induced spin relaxation of a diffusively moving carrier in low dimensions: Implications for spin transport in organic semiconductors

V. V. Mkhitaryan and V. V. Dobrovitski

Phys. Rev. B **92**, 054204 — Published 24 August 2015

DOI: 10.1103/PhysRevB.92.054204

Hyperfine-induced spin relaxation of a diffusively moving carrier in low dimensions: implications for spin transport in organic semiconductors

V. V. Mkhitaryan and V. V. Dobrovitski
Ames Laboratory, Iowa State University, Ames, Iowa 50011, USA

The hyperfine coupling between the spin of a charge carrier and the nuclear spin bath is a predominant channel for the carrier spin relaxation in many organic semiconductors. We theoretically investigate the hyperfine-induced spin relaxation of a carrier performing a random walk on a d-dimensional regular lattice, in a transport regime typical for organic semiconductors. We show that in $d = 1$ and $d = 2$ the time dependence of the space-integrated spin polarization, $P(t)$, is dominated by a superexponential decay, crossing over to a stretched exponential tail at long times. The faster decay is attributed to multiple self-intersections (returns) of the random walk trajectories, which occur more often in lower dimensions. We also show, analytically and numerically, that the returns lead to sensitivity of $P(t)$ to external electric and magnetic fields, and this sensitivity strongly depends on dimensionality of the system ($d = 1$ vs. $d = 3$). Furthermore, we investigate in detail the coordinate dependence of the time-integrated spin polarization, $\sigma(\mathbf{r})$, which can be probed in the spin transport experiments with spin-polarized electrodes. We demonstrate that, while $\sigma(\mathbf{r})$ is essentially exponential, the effect of multiple self-intersections can be identified in transport measurements from the strong dependence of the spin decay length on the external magnetic and electric fields.

PACS numbers: 72.25.Dc, 75.76.+j, 85.75.-d

I. INTRODUCTION

Spin dynamics of the charge carriers in organic semiconductors have attracted much attention recently[1–11]. On one hand, the processes which underlie the use of these systems in the organic light-emitting diodes and organic photovoltaic solar cells, are explicitly spin-dependent, so that understanding of the spin dynamics in organic semiconductors is of fundamental interest for such applications. On the other hand, the long spin lifetimes of the carriers in the organic semiconductors make them an interesting candidate for prospective spintronic applications, and the detailed understanding of the mechanisms of the spin relaxation is required.

Typically, charge transport in organic semiconductors occurs via random (incoherent and inelastic) hopping of the polarons carrying positive or negative charge between localized molecular sites. During the waiting time between two consecutive hops the carrier spin interacts via hyperfine coupling with the spins of the nuclei (mostly, hydrogen), which surround the host site. Thus, the spin of the carrier waiting for the next hop undergoes rotation around a random axis by a random angle at each site. The principal role of this mechanism was experimentally confirmed[6] and supported by a number of spin transport[5,12] and spin resonance[1,13,14] measurements, as well as theoretical works.[15–18] Another source of spin relaxation is the spin-orbit interaction, which leads to the spin-flip scattering in the course of a hop, but this interaction in organic semiconductors is weak, so the hyperfine-induced spin relaxation is likely to be the main source of depolarization, although other theoretical[19] and experimental[3,11] studies favor the spin-orbit mechanism, and theoretical efforts are made to explain this controversy.[20]

Spin dynamics of the polarons in low-dimensional systems is of particular interest: in the polymer-based devices the carriers mostly move along the 1D polymer chains, while hopping from one polymer chain to another happens mostly at the intersections. One-dimensional organic polymer wires can be prepared and their properties can be studied in detail, see e.g. Refs. 21,22. Also, engineering low-dimensional systems is a promising way to design organic materials with large magnetoresistance,[23] which are of much technological interest.

This motivates the theoretical study, described below, of the hyperfine-induced spin relaxation of a carrier diffusing via random walk in $d = 1$ and $d = 2$ dimensions. We investigate in detail not only the (space-) integrated spin polarization $P(t)$ (which has been addressed in some previous works[18,24–26]), but also the time-integrated polarization $\sigma(\mathbf{r})$ at the given point $\mathbf{r}$ in space, which can be measured in spin-transport experiments.[2–11,27] We show that for low-dimensional transport, these two quantities are related to each other in a rather non-trivial way. Moreover, we analyze the spin decay length l_S for $d = 1$ and $d = 2$, and show that it is very sensitive to both electric and magnetic fields; this is important both for applications and for the fundamental studies of the transport in organic semiconductors.

The average polaron hopping rate ν, corresponding to typical mobilities of 10^{-8} to 10^{-6} $\mathrm{cm^2V^{-1}s^{-1}}$, is of the order of 1–100 GHz.[28] At the same time, the average hyperfine-induced spin precession frequency is of order 100 MHz.[6,15] Therefore, the hopping is much faster than the hyperfine precession, and the carrier performs many random-walk steps before its spin polarization averages out to zero. Thus, the spin relaxation should be sensitive to the statistics of the underlying random walk. The particularly important feature of the random walk is the

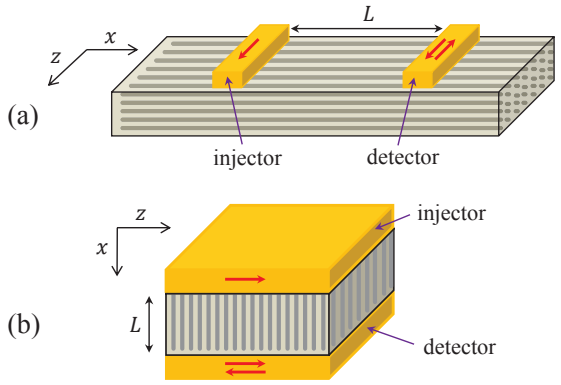

FIG. 1: (Color online) Lateral (a) and vertical (b) spin valves with organic active layer (gray), in which the charge carriers are restricted to move in one-dimensional channels along the x-direction. The separation between the injecting and detecting electrodes is L.

frequency of returns of the hopping carrier to the same site, i.e. the frequency of the self-intersections of the random walk trajectories. When the returns are absent, in the so-called transient diffusion regime[29], the random hyperfine field acting on the carrier's spin has no memory: the local hyperfine environments at different sites are uncorrelated, and the carrier hops from one site to another never coming back. This corresponds to the motional narrowing regime of the spin relaxation[30] and leads to the exponential decay of the space-integrated spin polarization, $P(t) \propto \exp(-t/t_{S,\mathrm{tr}})$, where $t_{S,\mathrm{tr}}$ is the spin relaxation time for the transient-diffusion regime[31,32]. The opposite scenario with frequent returns, known as the persistent diffusion, takes place when the carriers move in low-dimensional systems. The frequent returns to the same site lead to the random hyperfine field with long memory (long-time correlations), which suppresses the motional narrowing and leads to faster spin relaxation. The role of the memory of the hyperfine field has been studied for some scenarios, and has been found to change the spin relaxation of the spin polarization in $d = 1$ case to $P(t) \propto \exp\left[-(t/t_{S,1})^{3/2}\right]$ at short times[18,24–26], with the decay time $t_{S,1}$ depending on the particular model for the hyperfine fields. Also, it has been noticed that the returns make $P(t)$ very sensitive to the external magnetic field.[18]

However, the detailed knowledge about the carrier's spin relaxation in the case of low-dimensional transport is still largely lacking, and our work aims at filling this gap. We investigate analytically and numerically the spin relaxation for lateral and vertical spin valves (Fig. 1), with the carriers moving along the 1D current-carrying channels. We consider the limit of small current density, when each carrier moves independently of others, thus working within the single-particle framework. For the lateral spin valve, Fig. 1(a), the spin carrier hops along the very long linear chain, performing an unbounded random walk. For the vertical spin valve, Fig. 1(b), the random walk happens over finite-size chain with reflecting boundaries. In both cases we assume that the carrier is injected with the spin state "up" at $x = 0$, and its spin is probed by the detector at $x = L$.

We study the space-integrated spin polarization $P(t)$ and the time-integrated polarization $\sigma(\mathbf{r})$ at the given point $\mathbf{r}$, which can be measured with the detector lead at a given location. We demonstrate that these quantities exhibit remarkable universal features, and that the returns in the course of the carrier diffusion play an important role in this relation.

First, for the time decay of $P(t)$, we demonstrate the evidence of the universal scaling: for different values of the hyperfine coupling strength b_{hf} and hopping rate ν, the decay of $P(t)$ follows the same curve which depends only on the normalized dimensionless time $\tau = (\nu t)(b_{\mathrm{hf}}/\nu)^{4/3}$. This scaling holds not only for short times, where $P(t)$ follows the previously known decay law $P(t) = \exp\left[-(t/t_S)^{3/2}\right]$, but also at long times, where we find a previously unnoticed stretched-exponential decay $P(t) \sim \exp\left(-\alpha_1 t^{3/4}\right)$ (for both spin valve geometries). The scaling holds for both lateral and vertical spin-valve geometries, at zero magnetic and electric field. Also, we found that $P(t)$, besides the known sensitivity to the magnetic field, is also very sensitive to the electric field. We have observed the similarly strong effect of the returns for the spin relaxation in $d = 2$, leading to the logarithmic corrections to the standard exponential decay of $P(t)$, and strong sensitivity to the external fields.

Second, we studied the time-integrated polarization $\sigma(\mathbf{r})$, which is of much importance for the spin-dependent transport measurements. We are not aware of any analytical theory for this quantity, but our numerical studies reveal unexpected universality in its behavior. For persistent diffusion in low dimensions, in contrast to the transient diffusion in 3D, the quantity $\sigma(\mathbf{r})$ is not directly related to $P(t)$. Our numerical results show that, despite the essentially non-exponential decay of $P(t)$, the spin transport decay is exponential, $\sigma(r) \propto \exp(-r/l_S)$, with high accuracy, even in the presence of the external magnetic and electric fields. However, the resemblance to the usual 3D transient-diffusion result is superficial: for both $d = 1$ and $d = 2$ cases, the dependence of the spin decay length l_S on the external fields is very strong, in contrast to the standard 3D diffusion.

Our results suggest that the character of the carrier diffusion in an organic semiconductor can be studied in spin transport experiments, via the field dependence of l_S, and vice versa, the spin transport measurements in low-dimensional organic semiconductors can be used for accurate sensing of electric and magnetic fields, and for other similar spintronic applications.

The rest of the paper is organized as follows. In the next Section we discuss the formulation of the problem and the methods used for analytical and numerical studies. In Sections III and IV we consider the spin relaxation for the lateral and the vertical spin-valve geometries, respectively. Section V outlines our results on the spin

relaxation in $d = 2$. The effect of disorder in site energies is discussed in Section VI. Details of the analytical calculations are presented in two Appendices.

II. MODEL FOR THE CARRIER SPIN RELAXATION

We consider a carrier hopping between sites, see Fig. 2(a), which model organic molecules or conjugated segments of polymers. Everywhere below, for both $d = 1$ and $d = 2$, we enumerate sites by the integer variable $\mathbf{r}$, so that e.g. for 1D chain the physical coordinate of the site is $x = ar$, where a is the distance between the sites.

When the polaron is localized at the site with the radius-vector $\mathbf{r}$ its spin interacts with N nuclei $\mathbf{I}_{\mathbf{r}k}$ ($k = 1, .., N$) surrounding the given site. Below we assume that all nuclei have spin 1/2, since the protons in many organic semiconductors are the most abundant species with the largest nuclear magnetic moment. The Hamiltonian governing the spin dynamics of the carrier localized at the site $\mathbf{r}$ is:

$$H_{\mathbf{r}} = BS_z + \mathbf{S}\sum_{k=1}^{N} a_{\mathbf{r}k}\mathbf{I}_{\mathbf{r}k}, \tag{1}$$

where $a_{\mathbf{r}k}$ is the hyperfine coupling constant between the carrier spin and nuclear spin $\mathbf{I}_{\mathbf{r}k}$, and B is the Larmor frequency of the carrier spin $\mathbf{S}$ in an external magnetic field along the z axis (everywhere below we take $\hbar = 1$ and the electron's gyromagnetic ratio $\gamma_e = 1$, omitting the difference between the magnetic fields and the Larmor frequencies). Theoretical approach to the spin evolution in organic semiconductors customarily relies on the approximation where the quantum hyperfine field given by the sum in Eq. (1),

$$\hat{\mathbf{b}}_{\mathbf{r}} = \sum_{k=1}^{N} a_{\mathbf{r}k}\mathbf{I}_{\mathbf{r}k}, \tag{2}$$

is approximated as a static classical vector $\mathbf{b}_{\mathbf{r}}$ of random amplitude and direction, sampled from the Gaussian distribution with zero mean and the standard deviation equal to $b_{\rm hf} = \frac{1}{2}\sqrt{\sum_k a_{\mathbf{r}k}^2}$; this approximation is justified by the large number of nuclear spins coupled to the carrier spin at a given site (N of order 10 or more)[32–34]. We also assume that the hyperfine fields at different sites are uncorrelated, so that $\langle b_{\mathbf{r}}^{\alpha} b_{\mathbf{r}'}^{\beta}\rangle_{\rm hf} = b_{\rm hf}^2 \delta_{\alpha\beta}\delta_{\mathbf{r}\mathbf{r}'}$, where $\alpha, \beta = x, y, z$.

When we consider a carrier with the initial spin along $\hat{\mathbf{z}}$, performing a random walk with trajectory $\mathbf{r}(t)$, the carrier's spin $\boldsymbol{\mu}(t)$ evolves according to the equation of motion

$$\dot{\boldsymbol{\mu}} = \mathbf{b}_{\mathbf{r}(t)} \times \boldsymbol{\mu}(t) = \hat{\Omega}(\mathbf{r}(t))\boldsymbol{\mu}(t) \tag{3}$$

where the matrix

$$\hat{\Omega}(\mathbf{r}) = \begin{pmatrix} 0 & -b_{\mathbf{r}}^z & b_{\mathbf{r}}^y \\ b_{\mathbf{r}}^z & 0 & -b_{\mathbf{r}}^x \\ -b_{\mathbf{r}}^y & b_{\mathbf{r}}^x & 0 \end{pmatrix}, \tag{4}$$

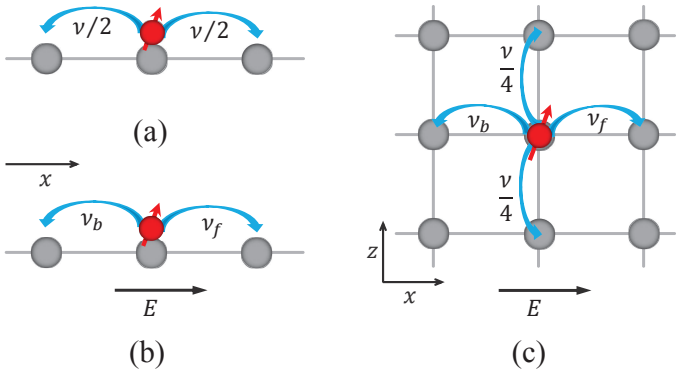

FIG. 2: (Color online) Diffusive random walk of a polaron (red circle) over $d = 1$ and $d = 2$ dimensional regular lattices of molecular sites (gray circles). (a) In the absence of external electric field, polaron hops between the nearest neighbor sites of $d = 1$ linear chain occur with the equal rates, $\nu/2$, indicated by the blue arrows. (b) In the presence of external electric field along the linear chain, hopping rates ν_f and ν_b, respectively in the directions forward and backward to the electric field, are different; $\nu_f > \nu_b$. (c) With an external electric field along the x axis of a regular lattice in $d = 2$, hopping rates in the forward and backward directions to $\hat{\mathbf{x}}$, ν_f and ν_b, can depend on the electric field, while the rates in the perpendicular direction are the same as without the field, and equal to $\nu/4$ each.

describes the spin rotation taking place at the site $\mathbf{r}$. Formal solution of this equation can be written in terms of the time-ordered exponent,

$$\boldsymbol{\mu}(t) = T\exp\int_0^t dt'\hat{\Omega}\big(\mathbf{r}(t')\big)\boldsymbol{\mu}(0),$$

with the initial condition $\boldsymbol{\mu}(0) = \hat{\mathbf{z}}$. The spin polarization is obtained by double averaging of the z-component of $\boldsymbol{\mu}(t)$,

$$P(t) = \langle\langle\mu^z(t)\rangle\rangle \equiv \left\langle\left\langle T\exp\int_0^t dt'\,\hat{\Omega}\big(\mathbf{r}(t')\big)\right\rangle_{\rm hf}\right\rangle_{\rm rw}\Big|_{zz}, \tag{5}$$

where $\langle\cdot\rangle_{\rm rw}$ denotes averaging over the random walk trajectories, $\langle\cdot\rangle_{\rm hf}$ denotes averaging over the local hyperfine fields, and the indices zz denote that we need to take the zz entry of the matrix which results after the averaging of the time-ordered matrix exponent.

Without returns, all spin rotations at different sites would be independent and uncorrelated, leading to exponential decay of the polarization as a function of time (the motional narrowing regime). In the presence of the returns, the rotations at different moments of time are correlated, and the polarization decay accelerates. In $d = 1$, the number of returns of the charge carrier to a given site after n hops is $\mathcal{O}\big(n^{1/2}\big)$, whereas in $d = 2$ and $d = 3$ this number is $\mathcal{O}\big(\ln n\big)$ and $\mathcal{O}\big(1\big)$, respectively.[35] Therefore one should expect that the influence of the returns is strong in $d = 1$, modest in $d = 2$, and weak in $d = 3$ dimensions; below we concentrate mainly on the $d = 1$ case where the effect is strongest.

The exact solution of Eq. (5) in the presence of returns is not available. In order to approach the problem, everywhere below we employ the fact that the hopping is much faster than rotation in the hyperfine field, so the parameter $\eta = b_{\rm hf}/\nu$ is small. Indeed, the value of $b_{\rm hf}$ is typically of order of 100 MHz, while the average carrier hopping rate ν is about 1–100 GHz, so

$$\eta = b_{\rm hf}/\nu \sim 0.1 - 0.001 \ll 1.$$

We can calculate $P(t)$ via the cumulant expansion in terms of the small parameter η:

$$P(t) = \left\langle\left\langle T\exp\int_0^t dt'\hat{\Omega}\big(\mathbf{r}(t')\big)\right\rangle\right\rangle\Big|_{zz} = \exp\left(\sum_n K_n(t)\right),$$

where $K_n(t)$ is proportional to η^n. The odd cumulants vanish (since the local Gaussian distributions of $\mathbf{b_r}$ have zero mean), the first non-vanishing cumulant $K_2(t)$ will determine the behavior of $P(t)$, at least at short times. We will demonstrate the accuracy of this approach by comparing the analytically calculated $K_2(t)$ with the results of the direct numerical simulations.

The numerical simulations are even more important for studying the time-integrated polarization $\sigma(\mathbf{r})$. We are not aware of any analytical theory for this quantity which would provide insights and guide our investigation. Thus, we rely solely on the numerical results, which demonstrate surprising and interesting universal features of $\sigma(\mathbf{r})$.

One could do numerical simulations by Monte-Carlo sampling of the random-walk trajectories and the distributions of the local fields, thus calculating the average in Eq. (5) directly. However, our results show that the statistical error is quite large, so instead we employ the approach based on the Liouville equation.

We describe the carrier spin via its density matrix $\rho_{\mathbf{r}}(t) = \frac{1}{2}\big(q_{\mathbf{r}}(t) + \mathbf{m_r}(t)\boldsymbol{\sigma}\big)$, where $q_{\mathbf{r}}(t)$ is the probability to find the carrier at site $\mathbf{r}$ at time t, and $\mathbf{m_r}(t)$ is its spin polarization; $\boldsymbol{\sigma}$ is the vector of Pauli matrices. The carrier dynamics obeys the master equation

$$\frac{dq_{\mathbf{r}}}{dt} = \sum_{\mathbf{r}'}\big[W_{\mathbf{r}',\mathbf{r}}q_{\mathbf{r}'}(t) - W_{\mathbf{r},\mathbf{r}'}q_{\mathbf{r}}(t)\big], \qquad (6)$$

where $W_{\mathbf{r},\mathbf{r}'}$ is the hopping rate from site $\mathbf{r}$ to $\mathbf{r}'$. At the same time, the spin polarization follows the generalized drift-diffusion equation,

$$\frac{d\mathbf{m_r}}{dt} = \sum_{\mathbf{r}'}\big[W_{\mathbf{r}',\mathbf{r}}\mathbf{m}_{\mathbf{r}'}(t) - W_{\mathbf{r},\mathbf{r}'}\mathbf{m_r}(t)\big] + \mathbf{b_r}\times\mathbf{m_r}. \quad (7)$$

For the charge carrier initially injected at the site $\mathbf{r} = 0$ in the spin-up state, the initial conditions correspond to $q_{\mathbf{r}}(0) = \delta_{\mathbf{r},0}$ and $\mathbf{m_r}(0) = \delta_{\mathbf{r},0}\mathbf{m}(0)$ with $\mathbf{m}(0) = (0,0,1)$ (directed along the z-axis). The solution $\mathbf{m_r}(t)$ of Eq. (7) includes averaging over the random-walk trajectories of the duration t, but the hyperfine fields at each site are taken as having some specific directions and amplitudes, i.e. the set $\{\boldsymbol{b}_{\mathbf{r}}\}$ of the local fields is fixed. Averaging over the local hyperfine fields is performed via Monte-Carlo sampling of $\{\boldsymbol{b}_{\mathbf{r}}\}$ at each site from the Gaussian distribution $\mathcal{N}(\mathbf{b}) = (2\pi b_{\rm hf})^{-3/2}\exp\big(-|\mathbf{b}|^2/2b_{\rm hf}^2\big)$. In particular, in this way we determine the time-integrated spin polarization at a given location,

$$\sigma(\mathbf{r}) = \nu\int_0^\infty dt\langle m_{\mathbf{r}}^z(t)\rangle_{\rm hf},$$

which plays an important role in the spin transport measurements.

We begin with considering carrier hopping between the nearest neighbor sites, with the equal hopping rates at each site (see Fig. 2). A disorder in the site energies, resulting in site-dependent hopping rates, will be considered in Section VI.

The effect of the external magnetic field is included into our model by simply adding the external field $\mathbf{B}$ to the local hyperfine fields. The external electric field E applied along the x-axis (Figs. 1 and 2) is taken into account by modifying the hopping rates: the hops along the field are more probable than backwards. Below, we assume, in the spirit of the Miller-Abrahams theory,[36] that the backward hopping rate ν_b (upwards in the electric field potential) is exponentially suppressed in comparison with the forward hopping rate ν_f (downwards in the electric potential), i.e. $\nu_b = (\nu/2)\exp(-\varepsilon)$, where $\varepsilon = eEa/k_BT$ with the Boltzmann constant k_B and temperature T, and eEa is the electric potential difference between two neighboring sites, while the forward-hopping rate remains unchanged, $\nu_f = \nu/2$. In particular, for $d = 1$, we have

$$\begin{aligned} W_{r,r'} &= (\nu/2)\,\delta_{r,r'-1} + (\nu/2)\,\delta_{r,r'+1} \quad \text{for } E = 0, \quad (8)\\ W_{r,r'} &= (\nu/2)\,\delta_{r,r'-1} + (\nu e^{-\varepsilon}/2)\,\delta_{r,r'+1} \quad \text{for } E \neq 0. \end{aligned}$$

III. SPIN RELAXATION IN A LATERAL SPIN VALVE

We neglect the effect of injector/detector electrodes, assuming insignificant tunneling between the leads and the semiconductor. For the lateral spin valve this implies unbounded diffusion over an infinite chain. For numerical simulations, we used a long chain with periodic or reflecting boundary conditions; the length was large enough to ensure vanishing population near the ends at all times. We also excluded from consideration the additional spin relaxation which is possible at the interface between a ferromagnetic electrode and an organic active layer[37–39].

A. $P(t)$ and $\sigma(r)$ in the absence of external fields

Important insights about the short-time behavior of $P(t)$ can be obtained analytically, using the lowest orders of the cumulant expansion in terms of the small

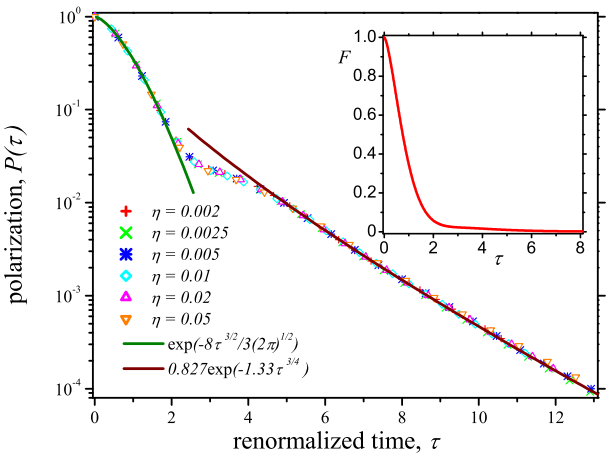

FIG. 3: (Color online) Logarithmic plot of $P(t)$ in $d = 1$, for values of $\eta \equiv b_{\rm hf}/\nu$ ranging from 0.002 to 0.05. When plotted against the renormalized time, $\tau = (\nu t)\eta^{4/3}$, all data points fall on a single scaling curve. The resulting scaling curve is well fitted by $\exp(-8\tau^{3/2}/3\sqrt{2\pi})$ for small τ and $0.827\exp(-1.33\tau^{3/4})$ for larger τ. Normal plot of the scaling curve, $F(\tau)$, is shown in the inset.

parameter $\eta = b_{\rm hf}/\nu$,

$$P(t) = \exp\left(\sum_n K_n(t)\right) \approx \exp\left[K_2(t)\right].$$

For a random walk over an infinite chain the first two non-vanishing cumulants, K_2 and K_4, are calculated in Appendix B. The second cumulant K_2 is determined by the two-time correlation function, $\langle\langle\hat\Omega(\mathbf{r}(t_1))\,\hat\Omega(\mathbf{r}(t_2))\rangle\rangle$. From the large-$t$ asymptotics of this correlation function we find:

$$K_2(t) \simeq -\frac{2\,b_{\rm hf}^2}{\sqrt{2\pi\nu}}\int\limits_0^t dt_1\int\limits_0^{t_1} dt_2\,\frac{1}{\sqrt{t_1-t_2}} = -\frac{8\,\eta^2(\nu t)^{\frac{3}{2}}}{3\sqrt{2\pi}}. \tag{9}$$

The next non-vanishing cumulant, K_4, is determined by the 4-th order correlation function of the process $\hat\Omega(\mathbf{r}(t))$. Our calculations in Appendix B show that it has small numerical prefactor, $K_4(t) \simeq 0.01\cdot\eta^4(\nu t)^3$, so that this cumulant becomes comparable to K_2 only at rather long times. Thus, $K_2(t)$ dominates the polarization decay at small times:

$$P(t) \approx e^{K_2(t)} = e^{-(t/t_S)^{3/2}}, \quad t_S = \frac{1}{\nu}\left(\frac{3\sqrt{2\pi}}{8\,\eta^2}\right)^{\frac{2}{3}}. \tag{10}$$

Excellent accuracy of this scaling at short times is seen from comparison with the direct numerical simulations in Fig. 3. The similar decay law, $P(t) \sim \exp(-t^{3/2})$, has been obtained in earlier studies, which assumed the single-axis local hyperfine fields (directed along the z-axis)[24–26], or the hyperfine fields with fixed amplitude randomly distributed in the x–y plane[18]. Our results confirm this decay law for the hyperfine fields distributed isotropically in space, and show that this feature holds for a very wide range of problems related to the spin decay during 1D diffusion; we will also see the same decay law below, for the vertical spin valve case.

More importantly, we notice that $K_2(t)$ and $K_4(t)$ depend only on the single dimensionless renormalized time $\tau = (\nu t)\eta^{4/3}$. From Eqs. (7) and (8) one can see that all cumulants, as well as $P(t)$ itself, are the functions of two dimensionless quantities, (νt) and η. However, our analytical and numerical studies evidence a much stronger result, that $P(t)$ is a function of a *single* dimensionless quantity τ. We performed a series of simulations for different values of η, and Fig. 3 shows that all results fall on the same universal curve $F(\tau)$, given in the inset of Fig. 3. This holds at all times we studied, even at large τ, when the contribution from the high-order cumulants is important.

Even more, we see that the same scaling holds when we consider the polarization decay at finite magnetic fields, finite electric fields, as well as for the case of the vertical spin valve (both without fields and with external magnetic and/or electric fields). Thus, it is highly likely that the renormalized time τ represents a universal feature of the spin decay for $d = 1$ random walk. Understanding of this remarkable scaling, as far as we know, is lacking.

Another interesting feature, seen from Fig. 3, is the decay of $P(t)$ at long times, which has a stretched-exponential form $P(t) \sim \exp\left(-\alpha\,\eta(\nu t)^{3/4}\right)$, with $\alpha = 1.33$; we checked that this form remains very accurate all the way down to $P(t) \sim 10^{-12}$. Again, to our knowledge, the reasons for this behavior are not understood yet.

Equally interesting is the behavior of the time-integrated polarization $\sigma(\mathbf{r})$. We are not aware of any analytical theory, which would provide insights in the behavior of this quantity and guide our simulations. Thus, we rely solely on the numerical results.

Our numerical simulations show that in the whole range of parameters $\sigma(r)$ has the exponential form, $\sigma(r) = l_S\exp(-|r|/l_S)$. Without external fields, the time-integrated polarization precisely follows the scaling law $\sigma(r) = \eta^{-2/3}G\left(r\eta^{2/3}\right)$, where the scaling function $G(w) = 0.68\exp(-1.47|w|)$ is obtained from numerical fitting. The origin of this scaling, as well as the origin of the exponential dependence of $\sigma(r)$, are not clear.

Note that the exponential decay of $\sigma(r)$ in the case of 1D persistent diffusion is not trivial. If multiple returns were negligible (as for transient diffusion in 3D), $P(t)$ would decay exponentially with the decay time $t_{S,\rm tr}$; the space- and time-integrated polarizations then would be related by the simple convolution[40], $\sigma(\mathbf{r}) = \nu\int_0^\infty dt P(t) q_{\mathbf{r}}(t)$, where $q_{\mathbf{r}}(t)$ is the probability to find the carrier at the site $\mathbf{r}$ at time t, see Eq. (6). The convolution would lead to the exponential decay $\sigma(r) = \exp(-|r|/l_{S,\rm tr})$ with the well-known diffusion relation $l_{S,\rm tr} = \sqrt{Dt_{S,\rm tr}}$, where D is the diffusion coefficient (for a random walk on a d-dimensional lattice, $D = \nu a^2/2d$,

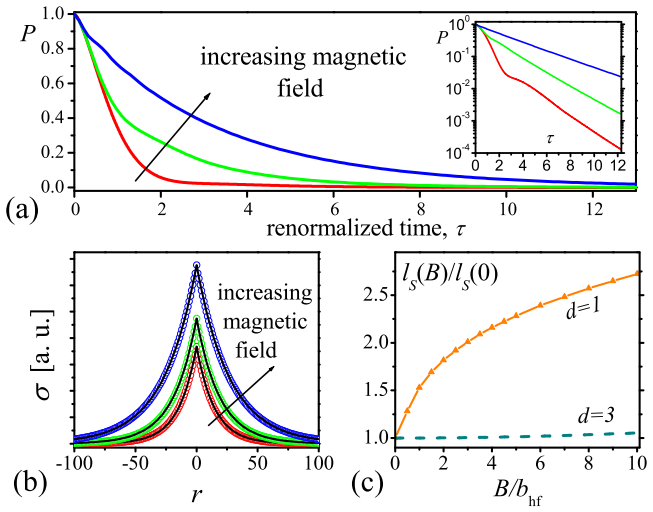

FIG. 4: (Color online) Magnetic field dependence of spin relaxation for a diffusion in $d = 1$ with $\eta = 0.01$. Red, green, and blue plots correspond to the magnetic field values $B = 0$, $0.5\,b_{\rm hf}$, and $2\,b_{\rm hf}$, respectively. (a) $P(t)$ is plotted against $\tau = (\nu t)\eta^{4/3}$; the red curve is the same as the one in the inset of Fig. 3. Inset: the same plot in the log-scale. (b) $\sigma(r)$ is plotted versus r. Black curves are our exponential fits. (c) The normalized spin decay length, $l_S(B)/l_S(0)$, is plotted vs $B/b_{\rm hf}$. Dashed line indicates $l_S(B)/l_S(0)$ without returns, plotted from Eq. (A13).

where a is the average distance between the sites).

However, in our case, where the returns are crucial, $\sigma(\mathbf{r})$ and $P(t)$ are not related in such a simple way, and it is not even clear whether such a relation exists. Indeed, if we used the same convolution of the non-exponential $P(t)$ with $q_{\mathbf{r}}(t)$ for 1D diffusion, we would obtain clearly non-exponential decay law for $\sigma(r)$. Thus, the origin of the exponential decay for $d = 1$ must be different from that of $d = 3$ case; this guess is supported by the qualitative difference in response of $P(t)$ and $\sigma(r)$ to the external magnetic and electric fields between the $d = 1$ and $d = 3$ cases.

B. Role of external magnetic field

It has been noticed previously[18] that in low dimensional diffusion, in the presence of multiple returns, $P(t)$ is very sensitive to the external magnetic field. For the magnetic field $\mathbf{B}$, the cumulant expansion of $P(t)$ can be carried out after applying the rotating-frame transformation, $\boldsymbol{\mu}(t) \to \exp(t\hat{\Omega}_B)\boldsymbol{\mu}(t)$, where $\hat{\Omega}_B$ is the skew-symmetric matrix formed of $\mathbf{B}$ (see Appendix B). Taking the external field as directed along the z-axis, we find the second cumulant

$$K_2^B(t) = -2b_{\rm hf}^2 \int_0^t dt_1 \int_0^{t_1} dt_2 \frac{\cos\big(B[t_1 - t_2]\big)}{\sqrt{2\pi\nu(t_1 - t_2)}}. \qquad (11)$$

It is instructive to compare Eqs. (11) and (9): the cosine term in the integrand is the only difference between the cumulants K_2 for zero magnetic field and K_2^B for finite magnetic field. This term induces a cutoff for $t \gtrsim B^{-1}$, reducing the integral significantly. This is somewhat similar to motional narrowing: because of the external magnetic field, the transversal components of the total field seen by $\boldsymbol{\mu}$ average out on the timescale B^{-1}.

Comparing Eqs. (10) and (11), one can see that the cutoff induced by the external magnetic field becomes important for $B \sim t_S^{-1} \sim \eta^{1/3} b_{\rm hf}$, which is even smaller than $b_{\rm hf}$. Our numerical results (Fig. 4) clearly verify this sensitivity already at very low fields. This behavior is in striking contrast with the transient diffusion in 3D, where the spin relaxation time would scale as $t_{S,\rm tr} \propto \big(1 + (B/\nu)^2\big)$, meaning that the magnetic field effects would be visible only at very large fields $B \sim \nu \gg b_{\rm hf}$.

The time-integrated spin polarization $\sigma(r)$ also exhibits strong sensitivity to the external magnetic field. It still has exponential form, $\sigma(r) \propto \exp\big[-|r|/l_S(B)\big]$, but the spin decay length sensitively depends on B; Fig. 4(b) illustrates this dependence for $\eta = 0.01$. The magnetic field dependence of the (normalized) spin decay length, $l_S(B)/l_S(0)$, is plotted in Fig. 4(c). Again, the analogy to the case of the transient 3D diffusion is superficial; this point is demonstrated in more detail in Appendix A [see Eq. (A13)], where the transient diffusion case is analyzed, and its qualitative difference with our results for $d = 1$ are emphasized.

C. Role of external electric field

If a drive voltage is applied to the spin valve (Fig. 1), the resulting electric field $\mathbf{E} = E\hat{\mathbf{x}}$ leads to a change in the hopping rates along and against the field direction (forward and backward hopping rates ν_f and ν_b, see Fig. 2(b)). Utilizing the Miller-Abrahams hopping model,[36] we take $\nu_b = (\nu/2)\exp(-\varepsilon)$, where $\varepsilon = eEa/k_BT$, and $\nu_f = \nu/2$ (independent of E). Overall, this would lead to slower motion of the carrier, implying slower changes of the random hyperfine field acting on it, and therefore (as it happens in the motional narrowing scenario) would produce faster decay of $P(t)$ with increasing ε. In the regime of 3D transient diffusion (see Appendix A for details) this is the most important effect: $P(t)$ would decay exponentially, and the decay time would decrease as $(\nu_f + \nu_b)/\nu$.

However, in the persistent-diffusion regime, the returns are important; besides inducing faster hopping, the electric field also changes the statistics of the returns. By making the forward hops more probable, the probability of the returns is decreased, thus profoundly affecting the

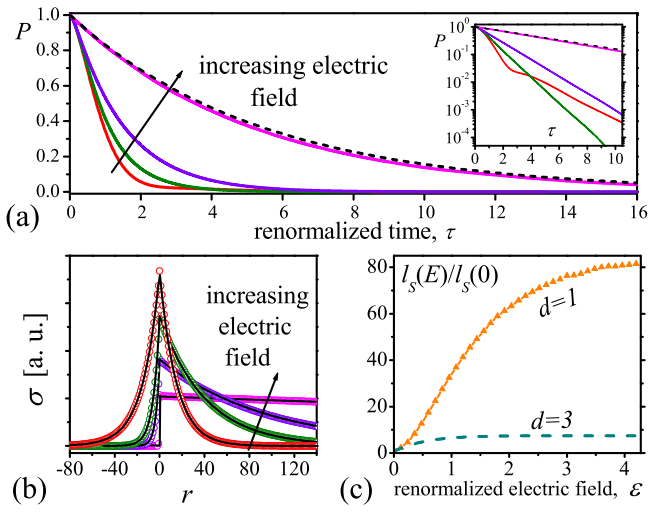

FIG. 5: (Color online) Electric field dependence of spin relaxation in $d = 1$ with $\eta = 0.01$, at zero magnetic field. With typical $a \approx 1$ nm and $T \approx 100$ K, parameter $\varepsilon \equiv eEa/k_BT$ corresponds to the electric field $E \approx 8.6\,\varepsilon$ mV/nm. The red, dark green, violet, and magenta plots correspond to $\varepsilon = 0$, 0.15, 0.3, and 3, respectively. (a) $P(t)$ is plotted versus $\tau = (\nu t)\eta^{4/3}$. The red curve is the same as in Fig. 4(a). The dashed black curve represents the exponential saturation for $\varepsilon \gg 1$. Inset: the same in the log-scale. (b) $\sigma(r)$ is plotted versus r. Black lines are our exponential fits. (c) Normalized spin decay length $l_S(\varepsilon)/l_S(0)$ versus ε (orange). The dashed line indicates the same dependence without multiple returns, plotted from Eq. (A16).

carrier spin relaxation. As above, we calculate the short-time behavior of $P(t)$ using the cumulant expansion, and the second cumulant in the presence of finite electric field is

$$K_2^E(t) = -b_{\rm hf}^2 \int_0^t dt_1 \int_0^{t_1} dt_2 \frac{e^{-(\sqrt{\nu_f}-\sqrt{\nu_b})^2[t_1-t_2]}}{(\nu_f\nu_b)^{1/4}\sqrt{\pi(t_1-t_2)}}. \qquad (12)$$

Here the exponent shows that the electric field prevents multiple returns. Because of the exponent, the integral in Eq. (12) mainly decreases with increasing E (see Appendix B for more details). This means that the spin relaxation slows down with increasing electric field, at least at relatively short times. The expected effect is seen in Fig. 5(a), which demonstrates simulation results for $P(t)$ for four different values of E.

In the limit of very high electric field, $\varepsilon \gg 1$, the carrier hops are all down-field, and the returns are blocked. In this limit one recovers the regime considered in Ref. 15, where the spin polarization decays exponentially. Specifically, to the leading order in large ε, the second cumulant is linear in time: $K_2^E(t) \approx -4\eta^2(\nu t)$ [see Appendix B for more details; note that the same result follows from the analytical calculations of spin relaxation without returns in Appendix A]. Therefore, as the electric field increases, the polarization $P(t)$ approaches the exponential form, as shown in Fig. 5. E.g., for $\eta = 0.01$ $P(t)$ is very close to the exponential form already at $\varepsilon = 3$.

Now we turn to the time-integrated spin polarization, $\sigma(r)$. Our numerical analysis shows that, like in all cases above, in the presence of finite electric field $\sigma(r)$ has exponential form, $\sigma(r) \propto \exp[-r/l_S(E)]$; see an example in Fig. 5(b) for $\eta = 0.01$. The curves are not symmetric with respect to $r = 0$, which is an obvious result of the drift induced by the electric field. Also note that, in contrast with two previous cases (no external fields and external magnetic field), the value of $\sigma(0)$, which sets the magnitude scale for the whole curve, is not proportional to $l_S(E)$ anymore, and decreases with increasing E, although $l_S(E)$ itself increases.

The spin decay length is very sensitive to the electric field: in Fig. 5(c) we show the dependence of $l_S(E)$ on the normalized electric field $\varepsilon = eEa/k_BT$ for $\eta = 0.01$, where $l_S(0) \approx 14.9$. This is to be contrasted with the similar dependence for a transiently diffusing carrier in $d = 3$ with the same $l_S(0)$, which is shown in the same graph for comparison: without returns, $l_S(E)$ shows much weaker changes with electric field.

IV. SPIN RELAXATION IN A VERTICAL SPIN VALVE

The geometry of the vertical spin valve, Fig. 1(b), suggests diffusion over a linear chain of a finite length L. Neglecting the back-tunneling into the electrodes, as it often happens in experiments, we obtain the perfectly reflecting boundaries. The spin relaxation now depends on the length of the system: $P(t) = P(t, L)$, $\sigma(r) = \sigma(r, L)$. Another feature of this geometry is that, instead of the whole function $\sigma(r, L)$, one is interested in its value at the detection electrode, $\sigma_*(L) \equiv \sigma(L, L)$.

A. $P(t)$ and $\sigma_*(L)$ in the absence of external fields

Let a carrier be implanted at the boundary site, $r = 1$, of a linear chain of finite length L. After n hops it will diffusively cover the distance $\sim \sqrt{n}$. With the hopping rate ν one has $n \approx \nu t$, so that for relatively short times, $\nu t < L^2$, the boundary at $r = L$ will not affect the spin relaxation noticeably. Therefore, for relatively short times, $P(t)$ can be found by considering a carrier diffusing over the semi-infinite chain, $r = 1, 2, ...$, with the reflecting boundary at $r = 1$. Calculation carried out in Appendix B for this case gives the second cumulant function,

$$K_2^{>}(t) \simeq -\frac{8\eta^2}{3\sqrt{\pi}}(\nu t)^{3/2}, \qquad (13)$$

which differs from K_2 of the infinite chain, Eq. (9), only by the factor $\sqrt{2}$. The ensuing short-time superexponential dependence of $P(t)$ is confirmed in our simulations, see Fig. 6.

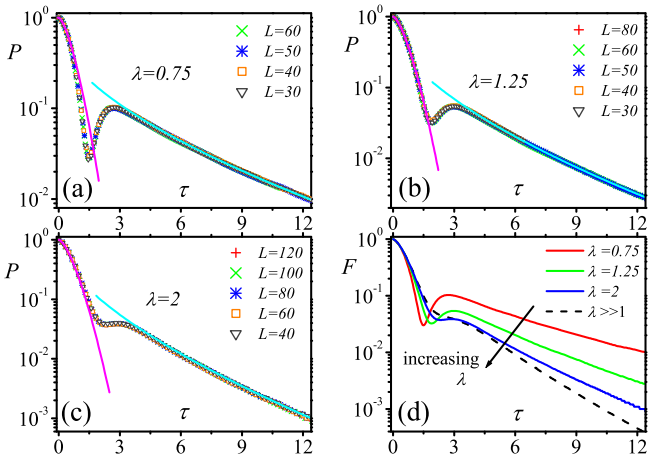

FIG. 6: (Color online) Spin relaxation in a finite chain of length L. When plotted versus $\tau = (\nu t)\,\eta^{4/3}$ and $\lambda = L\eta^{2/3}$, including (a) $\lambda = 0.75$, (b) $\lambda = 1.25$, and (c) $\lambda = 2$, all $P(t, L)$-points fall on universal curves. Cyan lines are stretched exponential fits, $P(t, L) \sim \exp(-\alpha t^{\beta})$, with (a) $\beta = 0.59$, (b) $\beta = 0.61$, and (c) $\beta = 0.64$. Magenta lines are our theoretical fits with $\exp(-8\tau^{3/2}/3\sqrt{\pi})$. (d) The resulting universal scaling function, $F(\tau, \lambda)$, is plotted for the above values of λ. The dashed line illustrates saturation of $F(\tau, \lambda)$ for $\lambda \to \infty$.

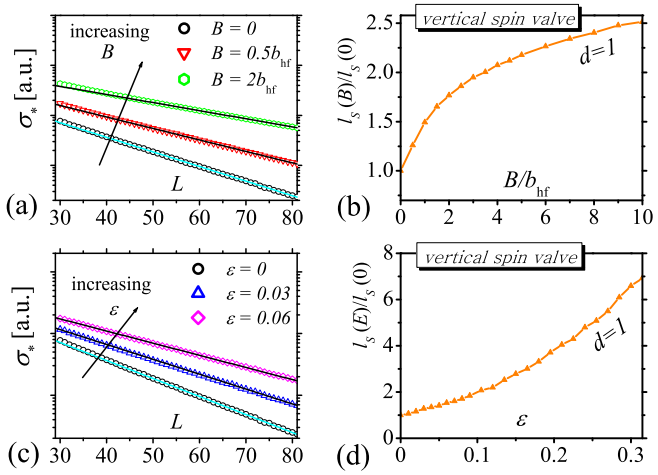

FIG. 7: (Color online) Spin polarization at the detection electrode, $\sigma_*(L)$, for a system with $\eta = 0.01$. (a) Log-plot of $\sigma_*(L)$ in zero electric field and different magnetic fields: $B = 0$ (black), $0.5\,b_{\rm hf}$ (red), $2\,b_{\rm hf}$ (green). (c) Log-plot of $\sigma_*(L)$ in three different electric fields, $\varepsilon = 0$ (black; the same as in (a)), $\varepsilon = 0.03$ (blue), $\varepsilon = 0.06$ (magenta), in zero magnetic field. The black and cyan lines in (a) and (c) are our exponential fits. (b) and (d): Dependence of the (normalized) diffusion length, $l_S/l_S(0)$, on external magnetic and electric fields, respectively.

At longer times, the influence of both boundaries becomes noticeable, and the decay of the spin polarization will depend on L. This dependence can be guessed using the results for unbounded diffusion given above.

As we have seen in the previous Section, the characteristic length of the spin relaxation is l_S, and scales with $\eta \equiv b_{\rm hf}/\nu$ as $\eta^{-2/3}$. Based on this fact and on Eq. (13), we can guess that the spin polarization should depend on the dimensionless time $\tau = (\nu t)\eta^{4/3}$ and on the dimensionless length $\lambda = L\eta^{2/3}$. Our numerical simulations confirm the expected scaling law $P(t, L) = F(\tau, \lambda)$, and provide the most notable features of the scaling function $F(\tau, \lambda)$. In Fig. 6 (a)–(c), we demonstrate the scaling by plotting $P(t, L)$ as a function of τ and λ, for three different values of λ and twelve different values of η.

These figures also show that the scaling function has the superexponential form $F(\tau, \lambda) = \exp(-8\tau^{3/2}/3\sqrt{\pi})$ at small times ($\tau \lesssim 0.5$), in accordance with Eq. (13), and is independent of the normalized chain length λ. At large times, the scaling function is accurately described by the stretched exponential, $F(\tau, \lambda) \sim \exp\bigl(-\alpha(\lambda)\tau^{\beta(\lambda)}\bigr)$, with the parameters which depend on the chain length; specifically, $\beta(0.75) = 0.59$, $\beta(1.25) = 0.61$, and $\beta(2) = 0.64$ in Figs. 6 (a)-(c), respectively. As the length of the chain increases, the exponent $\beta(\lambda)$ increases, saturating at the value $\beta = 0.75$ for very large λ that corresponds to the unbounded diffusion [see Fig. 6(d)].

In a similar way, we numerically verify the existence of scaling for the time-integrated spin polarization. As we expect, all length scales are scaled by the factor $\eta^{-2/3}$, so that $\sigma(r, L) = \eta^{-2/3} G\bigl(r\eta^{2/3}, L\eta^{2/3}\bigr)$, in analogy with the case of unbounded diffusion in the lateral spin valve. Correspondingly, for the spin polarization $\sigma_*(L)$, observed at the detector electrode, we have the scaling $\sigma_*(L) = \eta^{-2/3} G_*\bigl(L\eta^{2/3}\bigr)$. The numerical fitting shows that the scaling function is very accurately described as exponential, $G_*(w) = 2.712\exp(-1.475w)$. This corresponds to the dependence, $\sigma_*(L) = 4l_S\exp(-L/l_S)$, with the diffusion length, $l_S = 0.678\,\eta^{-2/3}$, which is nearly identical to the one found for the unbounded diffusion in the lateral spin valve.

B. Role of external magnetic and electric fields

In analogy with the case of the lateral spin valve, we studied the influence of the magnetic field $B\hat{\mathbf{z}}$ along the z-axis, and of the electric field $E\hat{\mathbf{x}}$ directed along the x-axis, on the spin relaxation.

We are primarily interested in the behavior of $\sigma_*(L)$. Our simulations (Fig. 7) show that it remains essentially exponential with L, in both external magnetic and electric fields. Thus, the field dependence of $\sigma_*(L)$ is fully encompassed by the field dependence of the spin decay length on B and $\varepsilon = eEa/k_BT$, shown in Figs. 7(b) and (d). As before, we see that the returns lead to strong sensitivity of l_S to the external fields, and this dependence is very close to its analog established in the previous Section. The curves in Figs. 7(b) and (d) appear to resemble the ones in Fig. 4(c) and Fig. 5(c).

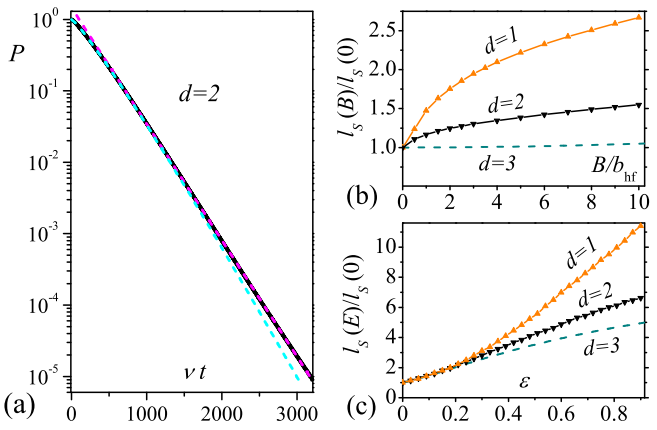

FIG. 8: (Color online) Spin relaxation of a carrier diffusing over $d = 2$ regular lattice, with $\eta \equiv b_{\rm hf}/\nu = 0.025$. (a) Log-plot of $P(t)$ against νt (black). The cyan dashed curve is plotted from Eq. (14). The magenta dashed line is our exponential fit. (b) Magnetic field dependence of the (normalized) spin decay length; $l_S/l_S(0)$ is plotted vs B for a diffusion in $d = 1$ with $\eta_1 = 0.021$ (orange), $d = 2$ with $\eta = 0.025$ (black), and strong-collision approximation to $d = 3$ with $\eta_3 = 0.032$ (dashed line). (c) Electric field dependence of the spin decay length. $l_S/l_S(0)$ is plotted vs $\varepsilon = eEa/k_BT$, for a diffusion in $d = 1$ with $\eta_1 = 0.021$ (orange), $d = 2$ with $\eta = 0.025$ (black), and $d = 3$ with $\eta_3 = 0.032$ in strong-collision approximation (dashed line).

V. SPIN RELAXATION IN $d = 2$

Above we focused on the analysis of the spin relaxation of a diffusing carrier for $d = 1$, mainly because the effect of multiple returns is strongest in this case. Meanwhile, it is rather straightforward to extend our analysis to the $d = 2$ case. For a carrier performing a simple random walk over a regular lattice in $d = 2$, the second cumulant function is calculated in Appendix B. It suggests the short-time decay

$$P(t) \simeq \exp\left[-2\,\eta^2(\nu t)\ln(\gamma\nu t)/\pi\right], \qquad (14)$$

where $\gamma = 5.243$ is a numerical coefficient. We have checked numerically that this formula accurately describes the spin relaxation down to rather small polarization values. Specifically, at $P(t) \sim 0.05$, the observed deviation from Eq. (14) was only about 0.002. Our simulations have also shown that at longer times the decay slows down, closely resembling exponential. This is shown in Fig. 8(a), which illustrates the spin relaxation in a system with $\eta = 0.025$. Thus, in $d = 2$ the effect of multiple returns is quite noticeable. Meanwhile, it is rather easy to check that in $d = 3$ the polarization decay is exponential at virtually all times.

To understand the spin-transport relaxation in $d = 2$, we consider a lateral spin valve device similar to that of Fig. 1(a), where the carriers hop between the sites of $d = 2$ regular lattice located in the x–z plane [see Fig. 2(c)], so that each site is characterized by the radius vector $\mathbf{r} = (x, z)$, with $x, z = 0, \pm1, \pm2, ...$ Assuming that the size of the organic layer in $\hat{\mathbf{z}}$-direction is much larger than the spin decay length, we characterize the spin-transport relaxation by the quantity,

$$\sigma_{2d}(x) = \sum_{\substack{\mathbf{r}=(x,z)\\ x=L}} \sigma(\mathbf{r}) \equiv \nu \sum_{\substack{\mathbf{r}=(x,z)\\ x=L}} \int_0^\infty dt \langle m_{\mathbf{r}}^z(t)\rangle_{\rm hf}, \qquad (15)$$

which is the total time-integrated spin polarization that has reached the detection electrode at $x = L$. Here $\mathbf{m}_{\mathbf{r}}(t)$ is the solution of drift-diffusion equation (7) for the 2D regular lattice; we solve this equation numerically, with the initial condition $\mathbf{m}_{\mathbf{r}}(0) = \delta_{\mathbf{r},0}\mathbf{m}(0)$. The influence of the external magnetic and electric fields is taken into account as described above.

Our results show that the decay of $\sigma_{2d}(x)$ is exponential, both with and without the external fields. The spin decay length l_S is also rather sensitive to the external fields, as a result of the returns in the course of the 2D random walk. This is illustrated in Figs. 8(b) and (c), where we compare the results for the random walk in different dimensions for $\eta = 0.025$, where the spin decay length in the absence of the external fields is $l_S = 9.0$. From the results of Section III one can see that the same zero-field spin decay length in $d = 1$ corresponds to $\eta_1 \approx 0.021$, whereas for $d = 3$, from the strong collision approximation (i.e., by neglecting multiple returns) we find the same zero-field spin decay length for $\eta_3 \approx 0.032$ [cf. Eq. (A13)]. Therefore, in Figs. 8(b) and (c) we compare the field dependence of the normalized spin decay length, $l_S(B)/l_S$ and $l_S(E)/l_S$, for $d = 1$ with $\eta_1 = 0.021$, $d = 2$ with $\eta = 0.025$, and $d = 3$ with $\eta_3 = 0.032$. Evidently, more frequently occurring multiple returns lead to stronger growth of spin decay length with external fields.

VI. EFFECT OF ENERGETIC DISORDER

In the previous Sections we have neglected the positional and energetic disorder of the molecular sites over which the hopping occurs. In this Section we consider the energetic disorder: it influences the dynamics of hopping by modifying the hopping rates, and the resulting changes in the diffusion lead to the changes in the spin relaxation. We do not consider the positional disorder, as it is believed to be much less important than the energetic one[41].

Earlier studies have demonstrated that the model with Gaussian distribution of the on-site energies often provides an adequate description for the charge transport in organic semiconductors[41–46]. In particular, the Gaussian model of disorder explained some aspects of the current relaxation[42,43], as well as the dependence of mobility on temperature and external electric field[41,44]. The typical spread of the on-site energies is of order of 0.1 eV, so

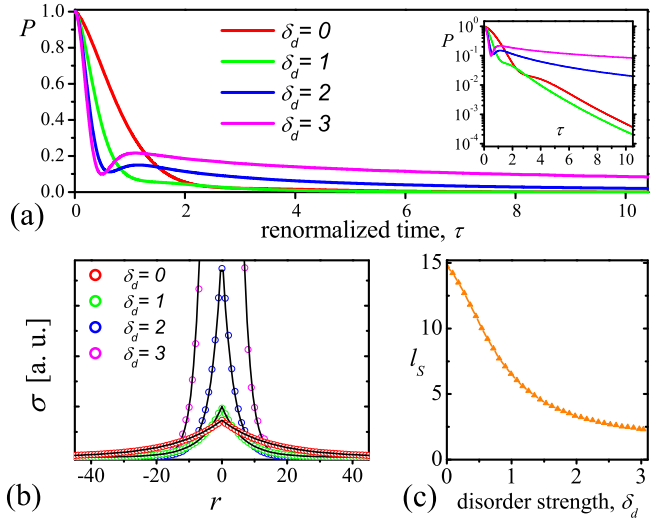

FIG. 9: (Color online) Spin relaxation in a 1D chain with Gaussian energetic disorder. Simulations are performed for a system with $\eta \equiv b_{\rm hf}/\nu = 0.01$, at zero magnetic and electric fields. The red, green, blue, and magenta plots correspond to $\delta_d = 0$, 1, 2, and 3, respectively. (a) $P(t)$ is plotted versus $\tau = (\nu t)\eta^{4/3}$. The red curve is the same as in Figs. 4(a) and 5(a). Inset: the same in the log-scale. (b) $\sigma(r)$ is plotted versus r. The black lines are exponential fits to the simulation results. (c) Dependence of the spin decay length l_S on the disorder strength δ_d.

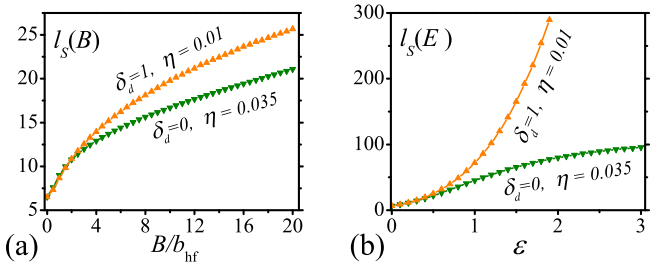

FIG. 10: (Color online) Dependence of the spin decay length on external magnetic and electric fields, in the presence of energy disorder. Plotted are the results for a system with energy disorder, $\delta_d = 1$, $\eta = 0.01$ (orange), and a system without energy disorder, $\delta_d = 0$, $\eta = 0.035$ (dark green). The systems are chosen to have the same zero-field spin decay length, $l_S(0) = 6.5$. (a) $l_S(B)$ is plotted versus $B/b_{\rm hf}$, at zero electric field. (b) $l_S(E)$ is plotted versus $\varepsilon \equiv eEa/k_BT$, at zero magnetic field. Disorder enhances the sensitivity of l_S to the external fields.

its effect can be noticeable at the normal experimental temperatures.

We use the Gaussian energetic disorder as the model for our studies, and, as in previous Sections, consider the carrier hopping rate given by the Miller-Abrahams model[36]. For convenience, we normalize the on-site energies by the Boltzmann factor k_BT. Thus, we assume that each site $r = 0, \pm1, \pm2, \ldots$ in the linear chain has a random (normalized) energy ϵ_r sampled from the Gaussian distribution

$$\mathcal{N}(\epsilon) = \frac{1}{\sqrt{2\pi\delta_d^2}} \exp\left(-\epsilon^2/2\delta_d^2\right),$$

and, the hopping rate from site r to site $r' = r \pm 1$ is

$$W_{r,r'} = \begin{cases} \nu \, \exp\left[-(\epsilon_{r'} - \epsilon_r)\right], & \epsilon_{r'} > \epsilon_r, \\ \nu, & \epsilon_{r'} < \epsilon_r, \end{cases} \qquad (16)$$

which coincides with Eq. (8) for $\delta_d = 0$.

We analyze the spin relaxation by numerically solving Eq. (7) in the same way as described in previous Sections, but now taking the random hopping rates caused by the energetic disorder, and performing additional averaging over this disorder. The simulation results for the system with $\eta = 0.01$ are illustrated in Fig. 9. The time decay of $P(t)$ remains superexponential at short times and stretched-exponential at long times. With the increasing disorder, the short-time decay of $P(t)$ becomes faster. The long-time decay, on the other hand, becomes slower for strong disorder, as seen in Fig. 9(a).

To understand these results, let us recall that the energetic disorder leads to a narrower, non-Gaussian spread of the carrier distribution (anomalous diffusion), with the mean square displacement sublinear in time[41,42,44], which means that the carrier spends more time near the origin with increasing disorder. The corresponding behavior of $P(t)$, shown in Fig. 9, is exactly what has been seen for the vertical spin valves in Sec. IV as a function of the system size: in both cases, the initial decay of $P(t)$ is faster and the long-time decay of $P(t)$ is slower for smaller systems, i.e. for the systems where the carrier spends more time near the origin.

Next we study the time-integrated spin polarization $\sigma(r)$ in the presence of disorder, and find that it remains exponential for all values of δ_d, see e.g. Fig. 9(b). With increasing disorder, the spin polarization becomes more localized in space. The spin decay length decreases with δ_d, see Fig. 9(c). At the same time, the overall magnitude of the spin polarization near the origin grows dramatically. This corresponds to the slow long-time decay of $P(t)$. Thus, although the energetic disorder leads to longer spin coherence times, the spin polarization becomes more and more localized, i.e. the spin transport is less efficient.

We also explore the effect of the external magnetic ($\mathbf{B} = B\hat{\mathbf{z}}$) and electric ($\mathbf{E} = E\hat{\mathbf{x}}$) fields in the presence of disorder. We verify that $\sigma(r)$ remains exponential. Moreover, the spin polarization is even more sensitive to external fields in the presence of disorder. Fig. 10 shows the field dependence of the spin decay length of a system with $\delta_d = 1$ and $\eta = 0.01$, in comparison with the no-disorder case, with $\delta_d = 0$ and $\eta = 0.035$. The different values of η are chosen to give the same zero-field spin decay length, $l_S(0) = 6.5$. The comparison shows

that energetic disorder results in stronger sensitivity to the external fields.

VII. CONCLUSION AND DISCUSSIONS

We have investigated spin relaxation of a carrier performing a random walk on a lattice, with random magnetic fields at each site. This models spin relaxation in organic semiconductors, where the charge transport between the π-conjugated segments of molecules is incoherent, and where the carrier spin interacts with the hydrogen nuclear spins surrounding a segment. Due to relatively large number of surrounding nuclear spins and their slow dynamics, the on-site random magnetic fields are taken as static, and sampled from the Gaussian distribution. The width of the distribution reflects the strength of hyperfine coupling at each site. For the incoherent hopping we assumed a random walk with the constant transition rates.

To understand the effect of multiple self-intersections of random walks, we have focused on the motion in $d = 1$ dimensional infinite linear chain. A superexponential short-time decay of spin polarization, $P(t) \sim \exp(-\alpha_1 t^{3/2})$, was found analytically from the cumulant expansion. The numerical simulations confirmed the superexponential dependence, and showed that it changes to a stretched exponential at longer times. We have also analyzed the spin relaxation of a carrier diffusing over a linear chain of finite length, and established that the short-time relaxation is somewhat faster, $P(t) \sim \exp(-\sqrt{2}\alpha_1 t^{3/2})$, whereas the stretched exponential long-time decay becomes slower. As a consequence of the multiple returns, in all these cases $P(t)$ is highly sensitive to the external magnetic and electric fields. For a diffusion over $d = 2$ regular lattice, we have found the short-time behavior $P(t) \sim \exp(-\alpha_2 t \ln t)$, smoothly crossing over to the exponential long-time decay.

Due to its relevance for the spin transport experiments, we have investigated the spin relaxation in the space domain, considering the time-integrated spin polarization $\sigma(\mathbf{r})$. It was demonstrated that, despite the strongly non-exponential decay in time, the spin relaxation in space is essentially exponential, superficially similar to that of a carrier diffusing in $d = 3$. However, diffusion in lower dimensions shows much stronger sensitivity to the external electric and magnetic fields. Importantly, this property is robust against the Gaussian disorder of site energies, which is typical for organic semiconductors.

It is interesting to compare our findings about the 1D transport with the experimental measurements on conjugated polymers. These systems may manifest 1D-transport features, as the diffusive motion along polymer chains may dominate over the jumps between the chains. The experiments on organic spin valves have not yet provided, to our knowledge, a direct measure of spin polarization or its decay inside the organic material[2–11]. Therefore, we use the previously suggested theory[6,15]

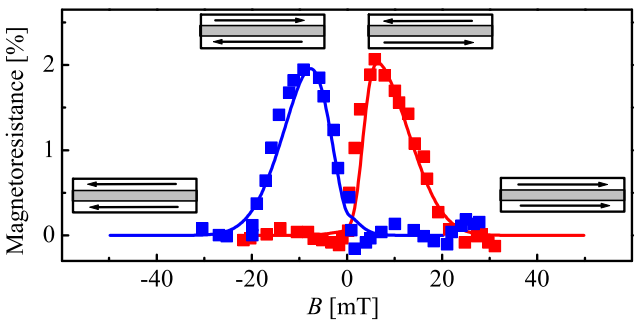

FIG. 11: (Color online) Fit of the magnetoresistance traces calculated from Eq. (17) [red and blue curves], to the experimental data from Fig. 4(a) of Ref. 6 [red and blue squares]. $l_S(B)$ is that shown in Fig. 10(a) in orange. Electrode coercive fields defining $m_{1,2}(B)$ are equal to those in Fig. 4(a) of Ref. 6: $B_{c1} = 3.3$ mT, $B_{c2} = 11$ mT. The curves are calculated at $b_{\rm hf} = 2$ mT and $d/l_S(0) = 1.54$. Insets show the magnetization orientations of the ferromagnetic electrodes.

which relates the field dependence of magnetoresistance $\mathrm{MR}(B)$ to the spin decay length $l_S(B)$ as

$$\mathrm{MR}(B) = \frac{1}{2}\mathrm{MR}_{\max}\big[1 - m_1(B)m_2(B)\big]\exp\big[-d/l_S(B)\big], \tag{17}$$

where $\mathrm{MR}_{\max}$ is the maximum magnetoresistance in the absence of spin relaxation, d is the effective separation between the electrodes, and $m_{1,2}(B)$ are the magnetizations of ferromagnetic electrodes normalized to their respective saturation magnetizations. Using the $l_S(B)$ dependence obtained above, see Fig. 10(a), we fit the calculated magnetoresistance traces to the experimental data of Ref. 6. Following the original work[6], the functions $m_{1,2}(B)$ were approximated as the error functions centered at the reported coercive fields of the Co and LSMO electrodes (3.3 mT and 11 mT, respectively); we found that the fit strongly depends not only on $l_S(B)$ but also on $m_{1,2}(B)$. The fitting results are shown in Fig. 11, which demonstrates good agreement between theory and experiment. While this initial result is encouraging, we expect that future experiments will provide data for more detailed and direct tests of our theory.

Acknowledgments

We thank J. Shinar and M. E. Raikh for many useful discussions. Work at the Ames Laboratory was supported by the US Department of Energy, Office of Science, Basic Energy Sciences, Division of Materials Sciences and Engineering. The Ames Laboratory is operated for the US Department of Energy by Iowa State University under Contract No. DE-AC02-07CH11358.

Appendix A

In this Appendix we calculate spin relaxation for a carrier diffusing transiently, i.e., when self-intersections of its random-walk trajectories are negligible, and the strong-collision approximation[47] is valid. Our starting point is Eq. (5) of the main text. Let $\mathbf{r}(t)$ be a random walk trajectory that starts at $\mathbf{r}_0 = 0$ and passes through n sites, $\mathbf{r}_1, .., \mathbf{r}_n$. Then the time-ordered exponent can be written as

$$T\exp\int_0^t dt'\mathbf{\Omega}(\mathbf{r}(t')) = e^{\tau_n\mathbf{\Omega}(\mathbf{r}_n)}\cdots e^{\tau_0\mathbf{\Omega}(\mathbf{r}_0)}, \qquad \text{(A1)}$$

where τ_k are the waiting time at $\mathbf{r}_k$, $k = 0, 1, .., n$. In the absence of self-intersections all $\mathbf{r}_k$ are different, and the average of Eq. (A1) over the local hyperfine frequencies is a product of exponents, averaged over the independent Gaussian distributions of hyperfine frequencies $\{\mathbf{b}_{\mathbf{r}_k}\}$, namely

$$\Big\langle T\exp\int_0^t dt'\mathbf{\Omega}(\mathbf{r}(t'))\Big\rangle_{\rm hf}\Big|_{zz} = \prod_{k=0}^{n} f(\tau_k), \qquad \text{(A2)}$$

where $f(\tau)$ is defined by $\langle e^{\tau\mathbf{\Omega}_\mathbf{b}}\rangle_{\{\mathbf{b}\}} = \hat{\mathbf{1}}f(\tau)$, with $\mathbf{\Omega}_\mathbf{b}$ being the skew-symmetric matrix formed of $\mathbf{b}$. By averaging

$$e^{\tau\mathbf{\Omega}_\mathbf{b}} = \hat{\mathbf{1}} + \sin(|\mathbf{b}|\tau)\frac{\mathbf{\Omega}_\mathbf{b}}{|\mathbf{b}|} + 2\sin^2(|\mathbf{b}|\tau/2)\frac{\mathbf{\Omega}_\mathbf{b}^2}{|\mathbf{b}|^2}, \qquad \text{(A3)}$$

over the Gaussian distribution of $\boldsymbol{b}$ with zero mean and standard deviation, $b_{\rm hf}$, one gets:

$$f(\tau) = \frac{1}{3} + \frac{2}{3}\big(1 - b_{\rm hf}^2\tau^2\big)\exp\big(-b_{\rm hf}^2\tau^2/2\big). \qquad \text{(A4)}$$

When a longitudinal magnetic field $\mathbf{B} = B\hat{\mathbf{z}}$ is applied, Eq. (A3) should be averaged over a Gaussian distribution of $\boldsymbol{b}$ with the mean, $\langle\mathbf{b}\rangle = B\hat{\mathbf{z}}$. Even though this leads to a non-diagonal matrix $\langle e^{\tau\mathbf{\Omega}_\mathbf{b}}\rangle_{\{\mathbf{b}\}}$, it remains block-diagonal, so that Eq. (A2) holds with a modified $f(\tau)$. Note in passing that $f(\tau)$ is a typical example of the static Kubo-Toyabe relaxation function.[47,48]

Next we want to average Eq. (A2) over the waiting time distributions and random-walk trajectories. Because of the absence of returns, the latter reduces to a summation over all n, whereas the former can be done by integrating $f(\tau)$ with the waiting-time distribution function, $\nu\, e^{-\nu\tau}$. Hence from Eqs. (5) and (A2) we get:

$$P(t) = \sum_{n=0}^{\infty}\int_0^\infty d\tau_0\cdots\int_0^\infty d\tau_n\prod_{j=0}^{n} f(\tau_j)\nu e^{-\nu\tau_j} \times\left[\theta\Big(t - \sum_{k=0}^{n-1}\tau_k\Big) - \theta\Big(t - \sum_{k=0}^{n}\tau_k\Big)\right]. \qquad \text{(A5)}$$

Here, the difference of θ-functions guarantees that at time t the walker has performed exactly n steps, so that $\sum_{k=0}^{n-1}\tau_k < t < \sum_{k=0}^{n}\tau_k$. Using the integral representation, $\theta(x) = \int\big[e^{izx}/(z - i\epsilon)\big]dz/(2\pi i)$, we reduce Eq. (A5) to

$$P(t) = \int_{-\infty}^{\infty}\frac{dz}{2\pi i}\frac{e^{iz\nu t}}{z - i\epsilon}\frac{u(1) - u(1 + iz)}{1 - u(1 + iz)}, \qquad \text{(A6)}$$

where $u(y) = \nu\int_0^\infty d\tau f(\tau)e^{-y\nu\tau}$. Going back to the definition of $f(\tau)$ ant taking the τ-integral we get:

$$u(y) = \frac{1}{y}\int d^3\boldsymbol{\zeta}\,\frac{e^{-\frac{|\zeta|^2}{2}}}{(2\pi)^{\frac{3}{2}}}\frac{(y\eta)^2 + (\zeta_z + \beta)^2}{(y\eta)^2 + \zeta_r^2 + \zeta_y^2 + (\zeta_z + \beta)^2}, \qquad \text{(A7)}$$

where $\beta = B/b_{\rm hf}$. Exact evaluation of this integral yields $u(y)$ in terms of the error function. However, we are interested in small values of $\eta \equiv b_{\rm hf}/\nu$, where the most relevant pole of Eq. (A6), given by $u(1 + iz_0) = 1$, is located at $|z_0| \ll 1$. Therefore z_0 can be found from the small-η ($\eta \ll \beta^{-1}$, 1) expansion of Eq. (A7) for $|y| \sim 1$,

$$u(y) \simeq \frac{1}{y}\left(1 - \frac{2}{(y/\eta)^2 + \beta^2 + 1}\right), \qquad \text{(A8)}$$

which in fact provides a good approximation for any β. Form Eq. (A8) we find $z_0 \approx 2i/(\eta^{-2} + \beta^2 + 1)$, yielding

$$P(t) \simeq e^{-t/t_S'}, \quad t_S' = (\eta^{-2} + \beta^2 + 1)/2\nu. \qquad \text{(A9)}$$

The spacial dependence of spin polarization is given by

$$\sigma(\mathbf{r}) = \nu\int_0^\infty dt\sum_{n=0}^{\infty}Q_n(\mathbf{r})\int_0^\infty d\tau_0\cdots\int_0^\infty d\tau_n\prod_{j=0}^{n} f(\tau_j)\nu e^{-\nu\tau_j} \times\left[\theta\Big(t - \sum_{k=0}^{n-1}\tau_k\Big) - \theta\Big(t - \sum_{k=0}^{n}\tau_k\Big)\right], \qquad \text{(A10)}$$

where $Q_n(\mathbf{r})$ is the probability that the random walker is at $\mathbf{r}$ after n steps. Calculating the integrals in Eq. (A10) is easy by taking first the t-integral. Further, introducing $\tilde{u} = \nu^2\int_0^\infty d\tau\tau f(\tau)e^{-\nu\tau}$ and using Eq. (A8), we find:

$$\sigma(\mathbf{r}) = \tilde{u}\sum_{n=0}^{\infty}Q_n(\mathbf{r})\big[u(1)\big]^n \simeq \sum_{n=0}^{\infty}Q_n(\mathbf{r})e^{-n/\nu t_S'}. \qquad \text{(A11)}$$

The probability $Q_n(\mathbf{r})$ is related to the solution of Eq. (6) as $q_\mathbf{r}(t) = e^{-\nu t}\sum_{n=0}^{\infty}Q_n(\mathbf{r})(\nu t)^n/n!$. This can be used in Eq. (A11) to express $\sigma(\mathbf{r})$ in terms of $q_\mathbf{r}(t)$:

$$\sigma(\mathbf{r}) \simeq \nu\int_0^\infty dt\, q_\mathbf{r}(t)P(t). \qquad \text{(A12)}$$

The large-r behavior of $\sigma(\mathbf{r})$ follows from that of $q_\mathbf{r}(t)$. Namely, for a simple random walk on a d-dimensional regular lattice one has $q_\mathbf{r}(t) = (2\pi\nu t/d)^{-d/2}\exp\big[-d|\mathbf{r}|^2/(2\nu t)\big]$, leading to the exponential decay, $\sigma(\mathbf{r}) \propto \exp\big(-|\mathbf{r}|/l_S\big)$, with

$$l_S(B) = \sqrt{\frac{\nu t_S'(B)}{2d}} \simeq \frac{1}{\sqrt{4d}\,\eta}\sqrt{1 + \big(\eta B/b_{\rm hf}\big)^2}. \qquad \text{(A13)}$$

In an external electric field, $\mathbf{E} = E\hat{\mathbf{x}}$, hopping rates along $\hat{\mathbf{x}}$ are changed. This leads to the drift along $\hat{\mathbf{x}}$, and also modifies the diffusion and the waiting-time distribution. While $P(t)$ is affected only because of the change in waiting-time distribution, $q_{\mathbf{r}}(t)$ and consequently $\sigma(\mathbf{r})$ are sensitive to the drift and diffusion. Assuming a random walk over a d-dimensional regular lattice, and for the hopping model considered in the main text, the hopping rates forward and backward to $\hat{\mathbf{x}}$ are $\nu_f = \nu/2d$ and $\nu_b = \nu e^{-\varepsilon}/2d$, where $\varepsilon = eEa/k_BT$, whereas in perpendicular directions hopping rates are $\nu/2d$. From the corresponding waiting-time distribution function, $\tilde{\nu}e^{-\tilde{\nu}\tau}$ with $\tilde{\nu} = \nu_f + \nu_b + \nu(d-1)/d$, one finds $P(t) \simeq \exp\bigl[-t/t'_S(\varepsilon)\bigr]$ with the electric-field dependent spin relaxation time,

$$t'_S(\varepsilon) = \frac{1}{2\nu\,\eta^2}\frac{2d-1+e^{-\varepsilon}}{2d} + \frac{\beta^2+1}{\nu}\frac{d}{2d-1+e^{-\varepsilon}}. \tag{A14}$$

The drift-diffusion equation (6) in $d = 3$ dimensions has the solution,

$$q_{\mathbf{r}}(t) = \left(\frac{\nu_f}{\nu_b}\right)^{\frac{x}{2}} e^{-\tilde{\nu}t} I_x\bigl(2\sqrt{\nu_f\nu_b}\,t\bigr) I_y\bigl(\nu t/d\bigr) I_z\bigl(\nu t/d\bigr), \tag{A15}$$

where $\mathbf{r} = (x, y, z)$ with $x, y, z = 0, \pm1, \pm2, ..,$ and I_α is the modified Bessel function of order α. For a spin valve similar to those illustrated in Fig. 1, we evaluate the quantity, $\sigma(x) = \sum_{y,z}\sigma(\mathbf{r})$ (in lower dimensions, one or both of last terms in Eq. (A15) should be eliminated, and the sum for $\sigma(x)$ should be changed correspondingly). After taking this sum, the integral Eq. (A12) reduces to the Laplace transform for a modified Bessel function, yielding $\sigma(x) \propto \exp\bigl[-x/l_S(\varepsilon)\bigr]$ for all $x > 0$, where

$$l_S(\varepsilon) = \frac{1}{\ln\left(\frac{1}{2}(1+e^{-\varepsilon}) + \frac{d}{\nu t'_S(\varepsilon)} + \sqrt{\left[\frac{1}{2}(1+e^{-\varepsilon}) + \frac{d}{\nu t'_S(\varepsilon)}\right]^2 - e^{-\varepsilon}}\right)}. \tag{A16}$$

This dependence is plotted in Fig. 5(c) for a system with $\beta = 0$ and $l_S(0) = 14.9$ (corresponding to $\eta = 0.0336$ in $d = 1$), and in Fig. 8(c) for a system with $\beta = 0$ and $l_S(0) = 9$ (corresponding to $\eta = 0.0322$ in $d = 3$).

Appendix B

In this Appendix we calculate the $d = 1$ dimensional second cumulant functions, K_2, K_2^B, K_2^E, $K_2^>$, Eqs. (9), (11), (12), and (13), the fourth cumulant function K_4, as well as the second cumulant for a simple random walk on a two-dimensional regular lattice, $K_2^{(2)}$. Basic ingredients of this calculation are the Markov property of random walk and its Greens function, $G(\mathbf{r}, \mathbf{r}', t)$, which is the solution of corresponding random walk equation (6) with the initial condition, $q_{\mathbf{r}'}(0) = \delta_{\mathbf{r},\mathbf{r}'}$. The second cumulant function of Eq. (5) is defined by

$$K_2(t) = \int_0^t dt_1 \int_0^{t_1} dt_2 \langle\langle \boldsymbol{\Omega}(t_1)\,\boldsymbol{\Omega}(t_2)\rangle\rangle_{zz}, \qquad \langle\langle \boldsymbol{\Omega}(t_1)\,\boldsymbol{\Omega}(t_2)\rangle\rangle \equiv \Bigl\langle\Bigl\langle \boldsymbol{\Omega}(\mathbf{r}(t_1))\,\boldsymbol{\Omega}(\mathbf{r}(t_2))\Bigr\rangle_{\rm hf}\Bigr\rangle_{\rm rw}, \tag{B1}$$

where the average over random walk trajectories and locally Gaussian hyperfine frequencies is meant. Using the matrix form, Eq. (4), and the fact that the components of $\mathbf{b}_{\mathbf{r}}$ are delta-correlated, $\langle b^\alpha_{\mathbf{r}}\, b^\beta_{\mathbf{r}'}\rangle_{\rm hf} = -b^2_{\rm hf}\delta_{\mathbf{r},\mathbf{r}'}\delta_{\alpha,\beta}$, one easily takes the average over local frequencies, resulting in $\langle\langle \boldsymbol{\Omega}(t_1)\,\boldsymbol{\Omega}(t_2)\rangle\rangle = -\hat{\mathbf{1}}\cdot 2\,b^2_{\rm hf}\,\langle\delta_{\mathbf{r}(t_1),\mathbf{r}(t_2)}\rangle_{\rm rw}$. For any type of random walk, this can be expressed via the Greens function as follows:

$$\langle\langle \boldsymbol{\Omega}(t_1)\,\boldsymbol{\Omega}(t_2)\rangle\rangle = -\hat{\mathbf{1}}\cdot 2\,b^2_{\rm hf}\sum_{\mathbf{r}} G(\mathbf{r}, \mathbf{r}, t_1 - t_2) G(0, \mathbf{r}, t_2). \tag{B2}$$

For the random walk on an infinite chain we have $G(r, r', t) = e^{-\nu t} I_{|r-r'|}(\nu t)$, where $I_r(z)$ is the modified Bessel function of order r. From Eq. (B2) we find, $\langle\langle \boldsymbol{\Omega}(t_1)\,\boldsymbol{\Omega}(t_2)\rangle\rangle_{zz} = -2\,b^2_{\rm hf} e^{-\nu(t_1-t_2)} I_0\bigl(\nu(t_1-t_2)\bigr)$, which gives the second cumulant,

$$K_2(t) = -2\,\eta^2 \int_0^{\nu t} dz_1 \int_0^{z_1} dz_2 e^{-(z_1-z_2)} I_0(z_1 - z_2). \tag{B3}$$

In view of large η, it is necessary to find the integral for large $(\nu t) \gg 1$. Utilizing the large-z asymptote $e^{-z} I_r(z) \simeq (2\pi z)^{-1/2} \exp\bigl(-r^2/2z\bigr)$ in the integrand, we arrive at the result Eq. (9).

As the odd cumulants are zero, the fourth cumulant function is expressed in terms of the four-time correlation function as follows:

$$\frac{1}{2}K_2^2(t) + K_4(t) = \int_0^t dt_1 \int_0^{t_1} dt_2 \int_0^{t_2} dt_3 \int_0^{t_3} dt_4 \langle\langle \mathbf{\Omega}(t_1)\, \mathbf{\Omega}(t_2)\, \mathbf{\Omega}(t_3)\, \mathbf{\Omega}(t_4)\rangle\rangle_{zz}. \tag{B4}$$

From Eq. (4) we find that the zz-component of the product $\mathbf{\Omega}(t_1)\, \mathbf{\Omega}(t_2)\, \mathbf{\Omega}(t_3)\, \mathbf{\Omega}(t_4)$ is equal to

$$b^z_{\mathbf{r}(t_2)} b^z_{\mathbf{r}(t_3)} \Bigl[b^x_{\mathbf{r}(t_1)} b^x_{\mathbf{r}(t_4)} + b^y_{\mathbf{r}(t_1)} b^y_{\mathbf{r}(t_4)} \Bigr] + \Bigl[b^x_{\mathbf{r}(t_1)} b^x_{\mathbf{r}(t_2)} + b^y_{\mathbf{r}(t_1)} b^y_{\mathbf{r}(t_2)} \Bigr] \Bigl[b^x_{\mathbf{r}(t_3)} b^x_{\mathbf{r}(t_4)} + b^y_{\mathbf{r}(t_3)} b^y_{\mathbf{r}(t_4)} \Bigr]. \tag{B5}$$

To find $\langle \mathbf{\Omega}(t_1)\, \mathbf{\Omega}(t_2)\, \mathbf{\Omega}(t_3)\, \mathbf{\Omega}(t_4)\rangle_{zz}$, we first average Eq. (B5) over the local hyperfine field distribution, then over the random walk trajectories. After the first averaging we get:

$$\langle \mathbf{\Omega}(t_1)\, \mathbf{\Omega}(t_2)\, \mathbf{\Omega}(t_3)\, \mathbf{\Omega}(t_4)\rangle_{zz} = b_{\rm hf}^4 \bigl\langle 4\, \delta_{\mathbf{r}(t_1),\mathbf{r}(t_2)} \delta_{\mathbf{r}(t_3),\mathbf{r}(t_4)} + 2\, \delta_{\mathbf{r}(t_1),\mathbf{r}(t_3)} \delta_{\mathbf{r}(t_2),\mathbf{r}(t_4)} + 4\, \delta_{\mathbf{r}(t_1),\mathbf{r}(t_4)} \delta_{\mathbf{r}(t_2),\mathbf{r}(t_3)} \bigr\rangle_{\rm rw}. \tag{B6}$$

This equation follows from the calculation of local field averages of the form, $\bigl\langle b^\alpha_{\mathbf{r}_1} b^\alpha_{\mathbf{r}_2} b^\beta_{\mathbf{r}_3} b^\beta_{\mathbf{r}_4} \bigr\rangle_{\rm hf}$. For $\alpha \neq \beta$, this calculation is simple and gives $b_{\rm hf}^4 \delta_{\mathbf{r}_1,\mathbf{r}_2} \delta_{\mathbf{r}_3,\mathbf{r}_4}$. For $\alpha = \beta$, on the other hand, it results in the combination, $b_{\rm hf}^4 \bigl(\delta_{\mathbf{r}_1,\mathbf{r}_2} \delta_{\mathbf{r}_3,\mathbf{r}_4} + \delta_{\mathbf{r}_1,\mathbf{r}_3} \delta_{\mathbf{r}_2,\mathbf{r}_4} + \delta_{\mathbf{r}_1,\mathbf{r}_4} \delta_{\mathbf{r}_2,\mathbf{r}_3} \bigr)$. Note that contributions with $\mathbf{r}_1 = \mathbf{r}_2 = \mathbf{r}_3 = \mathbf{r}_4$ cancel out from this combination due to the Gaussian character of local frequency distributions.

Next we average Eq. (B6) over the random walk trajectories. For a function of four coordinates, f, and times arranged as $t_1 \geq t_2 \geq t_3 \geq t_4$, from the Markov property of random walk one generally has:

$$\bigl\langle f\bigl(\mathbf{r}(t_1), \mathbf{r}(t_2), \mathbf{r}(t_3), \mathbf{r}(t_4)\bigr) \bigr\rangle_{\rm rw} = \sum_{\mathbf{r}_1,..,\mathbf{r}_4} f(\mathbf{r}_1, \mathbf{r}_2, \mathbf{r}_3, \mathbf{r}_4) G(\mathbf{r}_{12}, t_{12}) G(\mathbf{r}_{23}, t_{23}) G(\mathbf{r}_{34}, t_{34}) G(\mathbf{r}_4, t_4), \tag{B7}$$

where $\mathbf{r}_{ij} = \mathbf{r}_i - \mathbf{r}_j$ and $t_{ij} = t_i - t_j$. We apply Eq. (B7) with the infinite-chain Greens function to each term of Eq. (B6), and find the large- νt_{ij} asymptotes of the resulting quantities:

$$\bigl\langle \delta_{r(t_1),r(t_2)} \delta_{r(t_3),r(t_4)} \bigr\rangle_{\rm rw} = G(0, t_{12}) G(0, t_{34}) \simeq \frac{1}{2\pi\nu\sqrt{t_{12} t_{34}}}, \tag{B8}$$

$$\bigl\langle \delta_{r(t_1),r(t_3)} \delta_{r(t_2),r(t_4)} \bigr\rangle_{\rm rw} = \sum_r G(r, t_{12}) G(r, t_{23}) G(r, t_{34}) \simeq \frac{1}{2\pi\nu\sqrt{t_{13} t_{24} - t_{23}^2}}, \tag{B9}$$

$$\bigl\langle \delta_{r(t_1),r(t_4)} \delta_{r(t_2),r(t_3)} \bigr\rangle_{\rm rw} = G(0, t_{23}) \sum_r G(r, t_{12}) G(r, t_{34}) \simeq \frac{1}{2\pi\nu\sqrt{t_{14} t_{23} - t_{23}^2}}. \tag{B10}$$

Equations (B6) and (B8)-(B10) define the integrand of Eq. (B4). Using the asymptotic forms, we find:

$$\int_0^t dt_1 \int_0^{t_1} dt_2 \int_0^{t_2} dt_3 \int_0^{t_3} dt_4 \langle\langle \mathbf{\Omega}(t_1)\, \mathbf{\Omega}(t_2)\, \mathbf{\Omega}(t_3)\, \mathbf{\Omega}(t_4)\rangle\rangle_{zz} \simeq \frac{5}{9}\eta^4 (\nu t)^3. \tag{B11}$$

This relation, together with Eq. (B4), leads to the result,

$$K_4(t) \simeq \bigl[(5\pi - 16)/9\pi\bigr] \eta^4 (\nu t)^3. \tag{B12}$$

It is worthwhile to notice that Eqs. (B9) and (B10) make the non-Gaussian character of the stochastic process $\{\mathbf{\Omega}(t)\}$ explicit. Indeed, a Gaussian $\{\mathbf{\Omega}(t)\}$ would entail a factorization of four-time functions, as it happens in Eq. (B8), whereas Eqs. (B9) and (B10) do not satisfy this condition.

Consider now the spin polarization decay in $d = 1$, in the presence of a magnetic field along $\hat{\mathbf{z}}$. This case can be described by adding in Eq. (7) the term $\mathbf{B} \times \mathbf{m}_r$, where $\mathbf{B} = B\hat{\mathbf{z}}$. A straightforward evaluation of $\langle\langle \mathbf{\Omega}(t_1)\, \mathbf{\Omega}(t_2)\rangle\rangle$ by repeating the steps that have led from Eq. (B1) to Eq. (B3) is insufficient; magnetic field effects appear only in the fourth order, as a correction to K_4 of order $\sim \bigl(B b_{\rm hf}\bigr)^2$. Rather, a systematic expansion of $P(t)$ in powers of $b_{\rm hf}$ can be achieved after performing the rotating-frame transformation, $\mathbf{m}_r(t) = \exp(t\, \mathbf{\Omega}_B) \mathbf{n}_r(t)$. Then $\mathbf{n}_r(t)$ satisfies Eq. (7) with time-dependent local frequencies, $\tilde{\mathbf{b}}_r(t) = \exp(-t\, \mathbf{\Omega}_B) \mathbf{b}_r \exp(t\, \mathbf{\Omega}_B)$, and initial condition, $\mathbf{n}_r(0) = \delta_{r0} \mathbf{m}(0)$. Also, as $\exp(t\, \mathbf{\Omega}_B)$ does

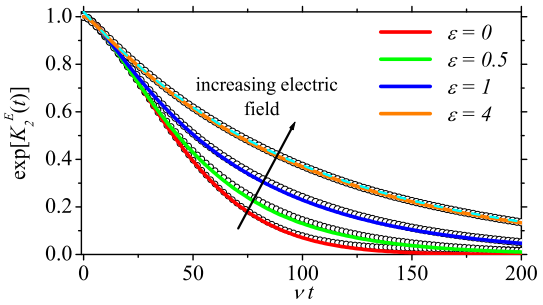

FIG. 12: (Color online) $\exp[K_2^E(t)]$ is plotted against (νt) from Eq. (B13) with $\eta = 0.05$, for $\varepsilon = 0$ (red), $\varepsilon = 0.5$ (green), $\varepsilon = 1$ (blue) and $\varepsilon = 4$ (orange). Open black circles are simulated points for $P(t)$ with corresponding values of parameters. The dashed cyan line indicates the large-ε asymptote, $\exp[-4\eta^2(\nu t - 2)]$.

not change the z-component of the vector on which it acts, $P(t)$ is expressed through $\mathbf{n}_r(t)$ exactly in the way it was in terms of $\mathbf{m}_r(t)$. Averaging over the distribution of local hyperfine fields now gives $\langle\langle \hat{\tilde{b}}(t_1)\,\hat{\tilde{b}}(t_2)\rangle\rangle_{zz} = -2\,b_{\rm hf}^2\cos\big(B[t_1-t_2]\big)\big\langle\delta_{r(t_1),r(t_2)}\big\rangle_{\rm rw}$, which leads to Eq. (11) after applying Eq. (B2) and large-(νt) expansion of the resulting Bessel function.

In the presence of electric field along $\hat{\mathbf{x}}$, the hopping rates forward and backward to $\hat{\mathbf{x}}$, ν_f and ν_b, are different. In the paper we utilize $\nu_f = \nu/2$, and $\nu_b = (\nu/2)e^{-\varepsilon}$. The diffusion propagator is given by $q_r(t) = (\nu_f/\nu_b)^{\frac{r}{2}}e^{-(\nu_f+\nu_b)t}I_r\big(2\sqrt{\nu_f\nu_b}\,t\big)$. This propagator leads to the second cumulant function,

$$K_2^E(t) = -2b_{\rm hf}^2\int\limits_0^t dt_1\int\limits_0^{t_1} dt_2 e^{-(\nu_f+\nu_b)[t_1-t_2]}I_0\big(2\sqrt{\nu_f\nu_b}[t_1-t_2]\big) \simeq -\frac{b_{\rm hf}^2}{(\nu_f\nu_b)^{1/4}}\int\limits_0^t dt_1\int\limits_0^{t_1} dt_2\frac{e^{-(\sqrt{\nu_f}-\sqrt{\nu_b})^2[t_1-t_2]}}{\sqrt{\pi(t_1-t_2)}}. \qquad \text{(B13)}$$

The E-dependence of $K_2^E(t)$ is non-trivial because the prefactor in Eq. (B13) grows as $\exp(\varepsilon/4)$, while the integral is suppressed with E. To clarify this dependence and to show that, for almost all t, the absolute value of the cumulant decreases with increasing E, we plot $\exp[K_2^E(t)]$ with $\eta = 0.05$ in Fig. 12, for three different values of E.

In the limit of large E ($\nu_b \to 0$), the form of $K_2^E(t)$ can be established from the first equation (B13) by using the asymptotic form of $I_0(z)$ for small arguments. For large number of hops, $(\nu t) \gg 1$, one finds the linear dependence, $K_2^E(t) \simeq -4\eta^2[(\nu t) - 2]$, so that the decay of $P(t)$ is predominantly exponential. This behavior is confirmed by our numerical simulations (see Fig. 12) and agrees well with that established in Ref. 15 in the same limit.

To find the cumulant function $K_2^{>}(t)$ for the case of a random walk over the semi-infinite chain, $r = 1, 2, ...$, with the reflecting boundary at $r = 1$, we exploit its Greens function, $G^{>}(r, r', t) = e^{-\nu t}\big[I_{|r-r'|}(\nu t) + I_{r+r'-1}(\nu t)\big]$. Plugging this Greens function in Eq. (B2) and using the large-νt expansion of the modified Bessel function yields

$$\langle\langle \mathbf{\Omega}(t_1)\,\mathbf{\Omega}(t_2)\rangle\rangle \simeq -\hat{\mathbf{1}}\cdot\frac{2\,b_{\rm hf}^2}{\sqrt{2\pi\nu}}\left(\frac{1}{\sqrt{t_1-t_2}}+\frac{1}{\sqrt{t_1+t_2}}\right). \qquad \text{(B14)}$$

By further integration we find the cumulant function Eq. (13).

The regular lattice in $d = 2$ can be described by the radius-vector, $\mathbf{r} = (x, y)$, with $x, y = 0, \pm1, \pm2, ...$, and $\hat{\mathbf{x}}$, $\hat{\mathbf{y}}$ along the lattice sides. The Greens function of the random walk over this lattice is $G^{(2)}(\mathbf{r}, \mathbf{r}', t) = e^{-\nu t}I_{|x-x'|}\big(\nu t/2\big)I_{|y-y'|}\big(\nu t/2\big)$. Further extension of Eqs. (B1)-(B3) to $d = 2$ is straightforward, leading to

$$K_2^{(2)}(t) = -2\,b_{\rm hf}^2\int\limits_0^t dt_1\int\limits_0^{t_1} dt_2\, e^{-\nu(t_1-t_2)}I_0^2\big(\nu(t_1-t_2)/2\big) = -2\,\eta^2\int\limits_0^{\nu t} dz(\nu t - z)e^{-z}I_0^2\big(z/2\big). \qquad \text{(B15)}$$

Combining numerical integration and asymptotic expansion of $I_0(z)$ for large z, we find the large-z expansion,

$$\int\limits_0^z dz'(z-z')e^{-z'}I_0^2\big(z'/2\big) = \frac{1}{\pi}z\ln(\gamma z) - \frac{1}{2\pi}\ln(z) + \zeta + \mathcal{O}(1/z), \qquad \gamma \approx 5.243, \quad \zeta \approx -0.264, \qquad \text{(B16)}$$

yielding

$$K_2^{(2)}(t) \simeq -2\eta^2(\nu t)\ln(\gamma\nu t)/\pi. \qquad \text{(B17)}$$

[1] J. Shinar, Laser Photonics Rev. **6**, 767 (2012).
[2] Z. H. Xiong, D. Wu, Z. V. Vardeny, and J. Shi, Nature (London) **427**, 821 (2004).
[3] S. Pramanik, C.-G. Stefanita, S. Patibandla, S. Bandyopadhyay, K. Garre, N. Harth, and M. Cahay, Nat. Nanotechnol. **2**, 216 (2007).
[4] A. J. Drew et al., Nat. Mater. **8**, 109 (2009).
[5] V. A. Dediu, L. E. Hueso, I. Bergenti, and C. Taliani, Nat. Mater. **8**, 850 (2009).
[6] T. Nguyen, G. Hukic-Markosian, F. Wang, L. Wojcik, X. Li, E. Ehrenfreund, Z. Vardeny, Nat. Mater. **9**, 345 (2010).
[7] M. Grünewald, M. Wahler, F. Schumann, M. Michelfeit, C. Gould, R. Schmidt, F. Würthner, G. Schmidt, and L. Molenkamp, Phys. Rev. B **84**, 125208 (2011).
[8] R. Lin, F. Wang, M. Wohlgenannt, C. He, X. Zhai, Y. Suzuki, Synth. Metals **161**, 553 (2011).
[9] M. Grünewald, R. Göckeritz, N. Homonnay, F. Würthner, L. W. Molenkamp, and G. Schmidt, Phys. Rev. B **88**, 085319 (2013).
[10] A. Riminucci, M. Prezioso, C. Pernechele, P. Graziosi, I. Bergenti, R. Cecchini, M. Calbucci, M. Solzi, and V. A. Dediu, Appl. Phys. Lett. **102**, 092407 (2013).
[11] S. Watanabe, K. Ando, K. Kang, S. Mooser, Y. Vaynzof, H. Kurebayashi, E. Saitoh, and H. Sirringhaus, Nat. Phys. **10**, 308 (2014).
[12] J. J. H. M. Schoonus, P. G. E. Lumens, W. Wagemans, J. T. Kohlhepp, P. A. Bobbert, H. J. M. Swagten, and B. Koopmans, Phys. Rev. Lett. **103**, 146601 (2009).
[13] H. Malissa, M. Kavand, D. P. Waters, K. J. van Schooten, P. L. Burn, Z. V. Vardeny, B. Saam, J. M. Lupton, and C. Boehme, Science **345**, 1487 (2014).
[14] D. R. McCamey, K. J. van Schooten, W. J. Baker, S.-Y. Lee, S.-Y. Paik, J. M. Lupton, and C. Boehme, Phys. Rev. Lett. **104**, 017601 (2010).
[15] P. A. Bobbert, W. Wagemans, F. W. A. van Oost, B. Koopmans, and M. Wohlgenannt, Phys. Rev. Lett. **102**, 156604 (2009).
[16] N. J. Harmon and M. E. Flatté, Phys. Rev. Lett. **108**, 186602 (2012).
[17] R. C. Roundy and M. E. Raikh, Phys. Rev. B **88**, 205206 (2013).
[18] R. C. Roundy and M. E. Raikh, Phys. Rev. B **90**, 201203 (2014).
[19] Z. G. Yu, Phys. Rev. Lett. **106**, 106602 (2011).
[20] N. J. Harmon and M. E. Flatté, Phys. Rev. Lett. **110**, 176602 (2013).
[21] G. Reecht, F. Scheurer, V. Speisser, Y. J. Dappe, F. Mathevet, G. Schull, Phys. Rev. Lett. **112**, 047403 (2014).
[22] R. N. Mahato, H. Lulf, M. H. Siekman, S. P. Kersten, P. A. Bobbert, M. P. de Jong, L. De Cola, and W. G. van der Wiel, Science **341**, 257 (2013).
[23] S. P. Kersten, S. C. J. Meskers, and P. A. Bobbert, Phys. Rev. B **86**, 045210 (2012).
[24] R. Czech and K. W. Kehr, Phys. Rev. Lett. **53**, 1783 (1984); Phys. Rev. B **34**, 261 (1986).
[25] P. Mitra and P. Le Doussal Phys. Rev. B **44**, 12035 (1991).
[26] P. Reineker and J. Köhler, Synth. Metals **43**, 3377 (1991).
[27] G. M. Akselrod, P. B. Deotare, N. J. Thompson, J. Lee, W. A. Tisdale, M. A. Baldo, V. M. Menon, and V. Bulović, Nat. Commun. **5** , 1 (2014).
[28] W. F. Pasveer, J. Cottaar, C. Tanase, R. Coehoorn, P. A. Bobbert, P. W. M. Blom, D. M. de Leeuw, and M. A. J. Michels, Phys. Rev. Lett. **94**, 206601 (2005).
[29] W. Feller, *An Introduction to Probability Theory and Its Applications*, Vol. I (John Wiley and Sons, New York, 2000).
[30] R. Kubo, J. Math. Phys. **4**, 174 (1963).
[31] R. G. Gordon, J. Chem. Phys. **44**, 1830 (1966).
[32] K. Schulten and P. G. Wolynes, J. Chem. Phys. **68**, 3292 (1978).
[33] S. I. Erlingsson and Yu. V. Nazarov, Phys. Rev. B **70**, 205327 (2004).
[34] K. A. Al-Hassanieh, V. V. Dobrovitski, E. Dagotto, and B. N. Harmon, Phys. Rev. Lett. **97**, 037204 (2006).
[35] E. W. Montroll and G. H. Weiss, J. Math. Phys. **6**, 167 (1965).
[36] A. Miller and E. Abrahams, Phys. Rev. **120**, 745 (1960).
[37] V. Dediu, M. Murgia, F. C. Matacotta, C. Taliani, and S. Barbanera, Solid State Commun. **122**, 181 (2002).
[38] M. Cinchetti, K. Heimer, J.-P. Wüstenberg, O. Andreyev, M. Bauer, S. Lach, C. Ziegler, Y. Gao, and M. Aeschlimann, Nat. Mater. **8**, 115 (2009).
[39] C. Barraud, P. Seneor, R. Mattana, S. Fusil, K. Bouzehouane, C. Deranlot, P. Graziosi, L. Hueso, I. Bergenti, V. Dediu, F. Petroff, and A. Fert, Nat. Phys. **6**, 615 (2010).
[40] Spin relaxation of a transiently diffusing carrier is calculated analytically in Appendix A, by neglecting the self-intersections of random walk trajectories.
[41] H. Bässler, Phys. Status Solidi B **175**, 15 (1993).
[42] P. M. Borsenberger, L. T. Pautmeier, and H. Bässler, Phys. Rev. B **46**, 12145 (1992).
[43] V. I. Arkhipov, I. I. Fishchuk, A. Kadashchuk, and H. Bässler, in *Photophysics of Molecular Materials: From Single Molecules to Single crystals*, edited by G. Lanzani (Wiley-VCH, Weinheim, 2006).
[44] L. Pautmeier, R. Richert, and H. Bässler, Synth. Met. **37**, 271 (1990).
[45] P. W. M. Blom and M. C. J. M. Vissenberg, Mater. Sci. Eng., R. **27**, 53 (2000).
[46] N. J. Harmon and M. E. Flatté, Phys. Rev. B **90**, 115203(2014).
[47] R. S. Hayano, Y. J. Uemura, J. Imazato, N. Nishida, T. Yamazaki, and R. Kubo, Phys. Rev. B **20**, 850 (1979).
[48] R. Kubo and T. Toyabe, in *Magnetic Resonance and Relaxation*, edited by R. Blinc (North-Holland, Amsterdam, 1967), pp. 810–823.